Reconstructing the geological evolution of small tropical volcanic islands: Insights from the study case of Moorea (French Polynesia)

T. Bechon, A. Hildenbrand, H. Pons, M. Dumont, P. Lachassagne, L. Sichoix

Journal of Volcanology and Geothermal Research 472 (2026) 108555

Contents lists available at ScienceDirect

Journal of Volcanology and Geothermal Research

journal homepage: www.journals.elsevier.com/journal-of-volcanology-and-geothermal-research

Reconstructing the geological evolution of small tropical volcanic islands: Insights from the study case of Moorea (French Polynesia)

T. Bechon [a], A. Hildenbrand [b], H. Pons [a,c], M. Dumont [d,e], P. Lachassagne [f], L. Sichoix [a,*]

[a] Laboratoire GEPASUD, Université de la Polynésie française, BP 6570, 98702, Faa'a, Tahiti, French Polynesia
[b] Laboratoire GEOPS, CNRS and Université Paris-Saclay, UMR8148, 91405, Orsay Cedex, France
[c] Education Nationale, France
[d] Hydrologic Science and Engineering Program, Colorado School of Mines, Golden, CO 80401, United States
[e] Institute of Earth Sciences, Université de Lausanne, Lausanne, CH-1015, Switzerland
[f] HSM, Université de Montpellier, CNRS, IRD, IMT Mines Alès, 34093, Montpellier, France

ARTICLE INFO

Keywords:
Volcanic island
Flank-collapse
Landslide
K/Ar dating
Moorea

ABSTRACT

Studying extinct volcanic islands is critical to constrain the geological evolution of intra-plate volcanoes and shed light on related natural hazards. From new fieldwork, geomorphological and new K/Ar geochronological data, we revisited the main stages of growth and destruction of Moorea, a small and highly eroded tropical volcanic island in French Polynesia. We show that: (1) the southern part of the island comprises the remnants of a main former basaltic volcano that was active between ca 1.85 Ma and 1.70 Ma; (2) the northern flank of this early edifice was removed around 1.64 Ma by a main flank-collapse that produced debris-avalanche partly exposed on the ocean floor up to 30 km from the island shore; the sudden subsequent decompression was followed by (3) vigorous volcanic activity witnessed by widespread strombolian deposits including peridotite xenoliths; a second main volcanic edifice rapidly grew inside the collapse depression between 1.64 Ma and ca 1.58 Ma, (4) overflowed into adjacent valleys until 1.50 Ma and (5) was followed by less-voluminous sporadic lava eruptions until ca 1.35 Ma; late volcanic units (3–5) were erupted from vents along the E–W direction, and/or small parasitic cones around the rims of the collapse scar; related lava flows covered unconformably the weathered slopes of the older edifice and filled existing paleo-valleys; (6) subsequent erosion enlarged the former landslide scar and led to significant topographic inversion. Successive construction and destruction episodes on small volcanic islands like Moorea led to strong geometric imbrication of geological units, which has important societal implications, e.g., for volcanic aquifers management or land occupation.

1. Introduction

Hotspot volcanic islands typically exhibit a complex history resulting from an alternation between constructive phases and destructive episodes (e.g.: Hildenbrand et al., 2004; Sibrant et al., 2015a,b). The latter may include large flank collapses, smaller landslides or other widespread erosional events (e.g., cliff retreat, river incisions, ...) which can produce the sudden release of significant amounts of debris (rock avalanches, lahars and concentrated flows) with potentially hazardous consequences (Keating and McGuire, 2000; Bret et al., 2003; Hildenbrand et al., 2008; Niyazi et al., 2025). Giant catastrophic flank collapses with individual volume exceeding 100 km^3 have been well-documented on large intra-plate volcanic islands worldwide, e.g., in Hawaii (Moore et al., 1989) and other islands in the Pacific (Clouard et al., 2001; Hildenbrand et al., 2006), in Réunion Island in the Indian Ocean (e.g.: Duffield et al., 1982; Gillot et al., 1994; Oehler et al., 2005), or in the Canary and Cape Verde archipelagoes in the Atlantic (e.g.: Carracedo et al., 1999; Masson et al., 2002, 2008; Boulesteix et al., 2013; Marques et al., 2019). More recently, less-voluminous events have been increasingly identified on smaller volcanic islands, especially those developed near major plate boundaries, e.g., in Stromboli (Casalbore et al., 2011), in the Caribbean (Le Friant et al., 2003; Dondin et al., 2012; Brunet et al., 2016), or in the Azores (Costa et al., 2014, 2015; Sibrant et al., 2015a,b; Hildenbrand et al., 2012, 2018, 2024; Marques et al., 2021, 2025). Such flank collapses may be triggered by a number of intrinsic and/or extrinsic factors including regional earthquakes, drastic pore-pressure increase generated by dyke intrusions along "rift-zones", changes in precipitation and sea level during major paleoclimatic events (see the 23 listed processes in Keating and McGuire, 2000; Quidelleur et al., 2008). Flank collapses usually occur during the main eruptive history

* Corresponding author.
E-mail address: lydie.sichoix@upf.pf (L. Sichoix).

https://doi.org/10.1016/j.jvolgeores.2026.108555
Received 30 July 2025; Received in revised form 23 January 2026; Accepted 29 January 2026
Available online 10 February 2026

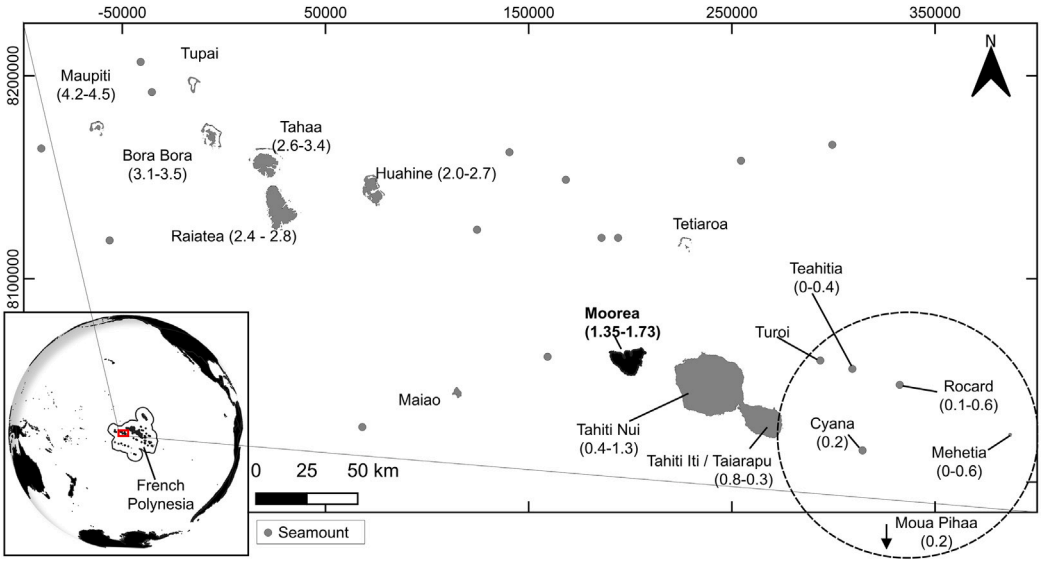

Fig. 1. Map of the society archipelago in French Polynesia (southern Pacific Ocean, see inset). Three remote atolls exist few hundred of kilometers west of Maupiti. The current hot spot sector is outlined with a dashed circle. Islands and atolls are shown. Seamounts are displayed as gray dots; some of them are probably missing due to the poor bathymetric resolution in some areas. Mehetia is a small island (not visible at this scale). Moorea is in black. Dates (in Ma) are from Le Roy (1994), Hildenbrand et al. (2004), Clouard and Bonneville (2005) and Guillou et al. (2005). The projected coordinate system is in EPSG:3297 (RGPF/UTM zone 6S), units are in meters.

of the volcanoes and result in the deep truncation of the feeding system. This triggers a sudden decompression, followed immediately by a subsequent massive eruptive response (Hildenbrand et al., 2004; Boulesteix et al., 2012). Consequently, the large scars left by these catastrophic events often lead to the infilling of the resulting depressions by newly emitted lava (e.g.: Hildenbrand et al., 2004; Boulesteix et al., 2012). However, after volcanic activity ceases and hundreds of thousands to several million years of erosion occur under a humid tropical climate with heavy rainfalls, on-land evidence of such dramatic events becomes increasingly scarce (Quesada-Román et al., 2025). Consequently, kilometer-scaled landslide structures have been often overlooked on many volcanic islands, especially in French Polynesia, in the absence of complementary data (e.g., acquired offshore). For instance, early geological maps of Tahiti-Nui (Deneufbourg, 1962; Brousse et al., 1985) report a simple conical volcanic edifice with a central sub-circular caldera that would have been created by vertical (piston-like) collapse. In contrast, more recent studies (Clouard et al., 2001; Hildenbrand et al., 2004, 2006) identified two-first order massive lateral flank collapses that were massively buried by post-collapse volcanism. The combination of offshore bathymetric Digital Elevation Model (DEM) analyses with extensive lava dating of on-land volcanic units has proven to be a valuable and effective approach to overcome such challenges.

We here revisit the geological and structural evolution of Moorea, a relatively small tropical volcanic island (ca. 15 km wide) west of Tahiti that has been inactive for the last 1.35 Ma (Fig. 1). With a current emerged area of 134 km^2, Moorea volcanic edifice has developed on a seafloor that descends to approximatively 3300–4300 m below present sea level. It exhibits a distinctive heart shape in plan view, and further shows an intriguing N–S topographic asymmetry. Yet, the island is believed to represent a unique main volcano that was affected in the north by either a sub-circular caldera, or a shallow listric fault (Le Dez, 1996; Le Dez et al., 1998; Maury et al., 2000). Over time, either gravitational processes and/or erosion have deeply incised the island, creating a highly contrasting topography characterized by steep cliffs and numerous canyons to wide valleys. While these deep erosive structures considerably modified the former volcanic morphology and obscured old volcanic structures, they constitute natural sections providing a unique opportunity to reach the various volcanic units and thus to reconstruct most of the island eruptive history. Here, we present a combination of new field structural/lithological observations acquired during an intensive survey (over 2 months cumulatively), 17 new high-precision K/Ar analyses on separated groundmass acquired on samples from the main volcanic units, and the use of open-source topographic and bathymetric datasets. These data allow us to reconstruct the main successive stages of growth and destruction of Moorea and to propose a new model of geological evolution that has significant societal implications (e.g.: water supply management, Lachassagne et al., 2014).

2. Geological and geodynamic background

Moorea is a small hotspot intraplate island belonging to the Society Archipelago in the southern Pacific Ocean (Fig. 1). It lies on the Pacific plate on a seafloor ca. 70 Ma in age (Clouard and Bonneville, 2005) and is neighboring the islands of Tahiti, Tetiaroa, and Maiao.

Moorea has a croissant-shaped topography with hundreds meters high cliffs dominated by several peaks (Fig. 2) such as Mt Tohiea (Th; 1207 m), Mt Mouaputa (Mpt; 830 m), Mt Tearai (Tr; 764 m), Mt Mouaroa (Mou; 880 m) and Mt Mouapu (Mp; 760 m). The concave side of the cliffs defines a main northern depression occupied by an isolated peak (Mt Rotui, 890 m). Gravimetric studies (Clouard et al., 2000; Shih et al., 2015) evidenced the presence of a positive density anomaly (dense inner magmatic system?), first in the middle of the depression (Clouard et al., 2000) or more recently shifted a few kilometers further east, close to the Mt Mouaputa side (Shih et al., 2015).

The geology of Moorea is dominated by volcanic deposits occurring mostly as lava flows and coarse-grained (poorly sorted) tephra layers formed by strombolian explosive eruptions. They range in composition from alkali basalts to quartz-bearing trachytes or trachyphonolites (Deneufbourg, 1962; Le Dez, 1996; Maury et al., 2000). Existing geochemical whole-rock data exhibit a compositional gap around 52 wt% in SiO_2 and around 7 wt% in alkali content. Magma evolution is dominantly referred to fractionated crystallization, but magma mixing between contrasted end-members was also proposed (Le Dez, 1996;

Maury et al., 2000). In a few places, plutonic rocks have also been reported by various authors: (1) gabbro boulders in the central depression or in two western valleys (Deneufbourg, 1962; Bellon and Blanchard, 1981; Le Dez, 1996; Guillou et al., 1998; Maury et al., 2000); (2) nodules of peridotites (dunite, wehrlite; Maury et al., 2000). Maury et al. (2000) observed large amounts of volcanoclastic detritic deposits (polygenetic breccias, lahars). They described an "unstratified, polygenetic breccia including more or less rounded basaltic blocks of variable texture [scoria to massive lava] in a brownish, clayey matrix, possibly cut by dykes", which encompasses various objects from different periods (syn- or post-volcanism) and of different origins (talus, debris flow and mud flow, see Bret et al., 2003). Other geological units include marine deposits comprising coral shelf, coral clasts and seashore conglomerate/sandstone (Deneufbourg, 1962; Maury et al., 2000). The various geological units have suffered variable weathering. The floor of the central depression of some valleys is covered by metric to a few decametric thick ferrallitic weathering cover (Jamet, 2000; Maury et al., 2000) resulting from the intense weathering of the protolith under a humid tropical climate.

The eruptive history of Moorea has been previously dated by K/Ar between ca 2 Ma and 1.35 Ma (Duncan and McDougall, 1976; Bellon and Blanchard, 1981; Diraison et al., 1991; Le Dez, 1996; Le Dez et al., 1998; Guillou et al., 1998, 2005; Maury et al., 2000; Uto et al., 2007). Those K/Ar datings were either acquired on whole-rock samples or on separated groundmass. As noted by several authors (e.g.: Quidelleur et al., 1999; Kelley, 2002; Guillou et al., 2005), the whole-rock approach often gives abnormal "too old" ages, due to the unsuitable incorporation of inherited excess-argon trapped in phenocrysts. For this reason, whole-rock K/Ar ages have to be discarded. Instead, K/Ar data on separated groundmass provides true eruption ages (see discussion in Gillot et al., 2006). On Moorea, previous K/Ar data on separated groundmass range between 1.72 ± 0.02 Ma and 1.36 ± 0.02 Ma (Le Dez, 1996; Le Dez et al., 1998; Guillou et al., 1998, 2005; Maury et al., 2000; Uto et al., 2007). Three main volcanic stages have been distinguished by these authors: (1) an old phase of unknown age (not dated by the authors), as inferred from basal laharic breccias comprising volcanic clasts, (2) a main shield phase between 1.72 Ma and 1.53 Ma; and (3) a late, post-shield phase represented by a few lavas and necks outcropping in the northern depression (Fig. 2) and two volcanic centers straddling on the eastern and western part of the fault. The creation of the northern depression and the singular position of Mt Rotui has been explained by two assumptions: (1) the vertical collapse of one or several calderas where the cliffs and outer slopes are residuals from the volcanic slopes (Deneufbourg, 1962; Guillou et al., 1998) or (2) a northward displacement of about 1000 m of the shield succession along a shallow listric fault (Le Dez, 1996; Le Dez et al., 1998; Maury et al., 2000). In both cases, the movement is believed to have occurred relatively late, as it affected the upper part of the main shield volcanic succession.

3. Methods

3.1. Geomorphological analysis and GIS

A Geographic Information System (GIS) was used before and during fieldwork to identify the main morphological characteristics, develop the sampling strategy, and report waypoints and observations. We merged two Digital Elevation Models (DEMs) with 5 m (full island cover) and 1 m (coastal cover) resolutions using QGIS software. These datasets are from the French governmental open source data repository (https://www.data.gouv.fr/datasets/modeles-numeriques-de-terrain-mnt-des-iles-de-la-polynesie-francaise/) and were produced by the "Cadastre-Topographie" section of French Polynesia. The DEM (5 m grid, same repository) of Tahiti was also exploited for the large-scale analysis (same source, used for Fig. 3).

For offshore bathymetry, two DEMs were used: one from the Hydrographic and Oceanographic Service of the (French) Navy (SHOM, 2023; https://diffusion.shom.fr/mnt-bathymetrique-de-facade-de-tahiti-et-moorea.html) with a 100 m grid spacing and another from the National Center for Environmental Information (NCEI), based on their Global Mosaic DEM available through the Bathymetric Data Viewer (https://www.ncei.noaa.gov/maps/bathymetry/, accessed in January 2025) with a ca. 90 m grid spacing. Given the limited knowledge of the submarine portion of the volcano, we opted to analyze the slope hillshade of the bathymetric DEM rather than relying solely on the elevation hillshade visualization. This approach was chosen to better highlight major underwater morphologies, which could be relevant to understand island-scale structures.

3.2. New geological investigations

Extensive fieldwork was conducted in most valleys, road-cuts and accessible pathways (see supplementary material S1). Observations aimed to identify the main volcanic successions and their first-order geometries. Further attention was paid to the nature and texture of individual deposits (lava flows, tephra, breccia) and their mutual relationships. The various structures and discontinuities (faults, dykes, paleosoils, unconformities, and lava tubes) were systematically mapped. Whenever possible, the rock type and the attitude (dip) of lava flows were reported. Throughout this article, the rock classification remains approximate, since bulk-rock compositions have not been analyzed. The denomination was based on color (leucocrate/melanocrate), texture (aphyric/porphyric) and identified minerals, either in the field or in thin sections, as well as K content.

Rock sampling strategy was focused on both the top and base of the main successions to constrain the age and duration of the main volcanic phases. We targeted areas that had been less studied in previous works — specifically the deepest parts of the southern valleys, and the NNE sector of the island. Additional sampling was conducted around the two main bays to reassess the currently proposed geological structure. Only lava flows were sampled for subsequent geochronological analyses. The inner massive (generally prismatic) parts were systematically detached with a chisel and hammer, and further broken with a sledge hammer to reach the freshest rock and remove superficial parts with obvious signs of weathering and/or extended zeolitization. We note, however, that a few lava flows showed significant penetrative weathering marked by an obvious reddish thick alteration profile (e.g.: MO24C). Even in those cases, the original structure of the lava flow was recognized, and the fresh massive lava core below the weathering front could be reached and sampled. Particular attention was paid to avoid sampling dykes as they may have preserved ^{40}Ar excess during instant cooling. Lava flows close to dykes were also avoided as they may have experienced partial re-setting of the geochronometer (argon diffusion) due to *in-situ* re-heating at the contact with thick intrusions.

3.3. K/Ar dating

Basic volcanic products of late Quaternary age can be dated using both K/Ar and $^{40}Ar/^{39}Ar$ techniques, but the latter can be challenging, as irradiation of such low-K and high-Ca samples in a nuclear reactor generates the unsuitable artificial production of Ar isotopes (especially ^{36}Ar from Ca), which needs to be corrected for, thereby increasing age uncertainty (e.g., Quidelleur and Famin, 2024). Furthermore, glassy samples such as lavas from Moorea may experience significant ^{37}Ar and ^{39}Ar argon loss by ejection-re-coil during irradiation processes, which may further bias accurate age determination (McDougall and Harrison, 1999; Schaen et al., 2020). In contrast, the K/Ar technique does not suffer such drawbacks as no irradiation of the samples is necessary. The peculiar unspiked K/Ar Cassignol–Gillot technique developed in GEOPS (University Paris-Saclay, France) has been shown especially suitable to measure reliable and precise eruption ages on low-K basalts and

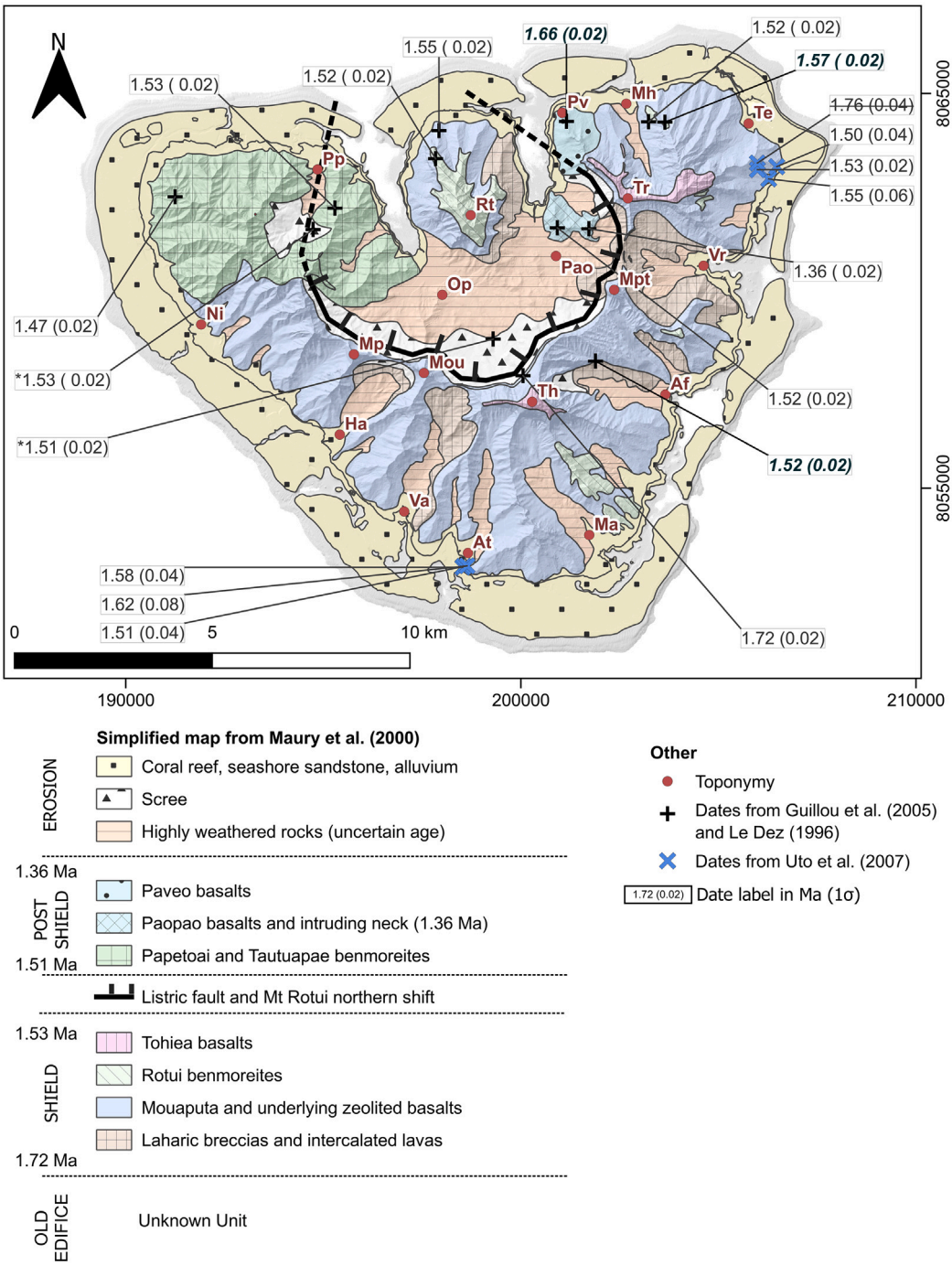

Fig. 2. Modified and simplified geological map from Maury et al. (2000), inspired by Guillou et al. (2005). Ages (Ma) from Le Dez (1996) were reported as long as the one from Uto et al. (2007). Three rocks dated by Guillou and removed from most of their further publications (Guillou et al., 1998, 2005; Maury et al., 2000) were taken from Le Dez (1996) or Le Dez et al. (1998); removed samples are represented in bold letters and will be discussed latter in the text. Samples with * were taken in screes assuming they belong to inaccessible lavas located high in the cliffs (Maury et al., 2000). One crossed-out date (1.76 Ma) from Uto et al. (2007) was suspected to have inherited Ar and was cast aside by the authors. Uncertainties, specified between brackets, represent the 1σ error. Local names are Afareaitu (Af); Atiha (At); Haapiti (Ha) ; Maatea (Ma); Maharepa (Mh); Mouaroa (Mou); Mouapu (Mp); Mouaputa (Mpt); Niumaru (Ni); Opunohu (Op); Paopao (Pao); Papetoai (Pp); Paveo (Pv); Rotui (Rt); Temae (Te); Tohiea (Th); Tearai (Tr); Vaianae (Va); Vaiare (Vr). The coordinate system is in EPSG:3297 (RGPF/UTM zone 6S), units are in meters.

andesites, down to sub-historical periods (Gillot et al., 2006). It has been widely used to constrain successfully the Quaternary evolution of many volcanic islands worldwide (Gillot et al., 1994; Hildenbrand et al., 2004, 2012; Germa et al., 2011a,b; Costa et al., 2015; Sibrant et al., 2015a,b; Ricci et al., 2020; Quidelleur and Famin, 2024; Rougeau et al., 2024). The unspiked Cassignol–Gillot technique appears the most suitable for the present study.

Thin sections were prepared for each sample to assess the quality of the groundmass and to determine the presence or absence of devitrification or secondary minerals. The remaining rock was sliced to facilitate

crushing using a diamond saw and the altered crust or labeling were previously removed.

The selected samples were crushed using an anvil, a hammer, and a steel piston. The crushed material was sieved to a size fraction of either 125–250 μm or 63–125 μm so as to eliminate major phenocrysts and avoid large vesicles (see online supplementary material S2 and S3 for sample description). After ultrasonication in a dilute nitric acid solution to neutralize organic matter and dissolve potential secondary minerals such as calcite and zeolites, the samples were thoroughly rinsed with de-ionized water and ethanol and dried in an oven at 60 °C.

Most phenocrysts (olivine, pyroxene, plagioclase) often contain excess argon (melt or fluid inclusions; Kelley, 2002), which may bias the determination of the eruption age. Thus, they were systematically discarded through a magnetic sorting and the systematic use of heavy liquids (diiodomethane and bromoform). The freshest part of the groundmass was selected in a narrow density interval, and checked under a binocular magnifier. When multiple density classes were deemed suitable for analysis, the densest among them was chosen to minimize the risk of glass devitrification.

K and Ar mass proportions were measured in the GEOPS lab on distinct aliquots of the same selected fresh and homogeneous sample preparation. For samples MO24J and MO24L, which contained some zeolites, two distinct density fractions were analyzed in order to test for internal consistency of the sample, and assess any secondary perturbation of the chronometer, e.g. due to K-loss by weathering processes.

The K-content was measured using flame absorption spectrophotometry using an Agilent 200 Series AA following the method described elsewhere (e.g.: Gillot et al., 2006). Samples were first attacked with HF (hydrofluoric acid) on a hot plate overnight to destroy the silicate network. Residues were dissolved in distilled water and HCl. To calibrate the spectrophotometer, standard solutions containing known concentration of K were prepared. BCR2 (basalt) and MDO-G (trachyte) international standards (Gillot et al., 1992; Raczek et al., 2001) were analyzed as unknown samples to ensure the consistency of the results. As for Ar, each K analysis was performed at least twice to ensure the reproducibility of the results. The $^{40}Ar/^{36}Ar$ measurements were performed on 0.8–2.5 g of sample, enclosed in a copper capsule and placed in a molybdenum crucible. We used the unspiked Cassignol–Gillot technique described in Gillot et al. (2006) which has been shown especially appropriate to date precisely low-K Quaternary basalts and andesites. The sample was inductively heated up to over 1200 °C under vacuum conditions of 10^{-7} to 10^{-8} Torr to fully melt the rock sample and release all volatiles contained in the rock. After trapping on active charcoal with liquid nitrogen, reactive gases were purified on hot titanium foam (around 850 °C), and further purified on three getters. Residual gases (He, Ar, Ne, Kr) were then introduced into a mass spectrometer to measure ^{36}Ar and ^{40}Ar.

Calibration of the ^{40}Ar signal in the mass spectrometer was achieved with an air pipette regularly checked from routine measurements on biotite standard HDB-1 with a recommended age of 24.18 Ma (Schwarz and Trieloff, 2007). After sample analysis, pure atmosphere with a similar ^{40}Ar signal was analyzed to calculate the amount of atmospheric contamination and deduce the amount of radiogenic ^{40}Ar ($^{40}Ar^*$). To ensure analytical reliability and eliminate systematic biases, all runs were replicated using different setup configurations (e.g., alternative furnaces, varied sample orders, and different measurement days).

Age uncertainty (1σ) is reported as the quadratic sum of all sources of relative uncertainties: K (1%), Ar calibration (1%), and uncertainty on the atmospheric contamination (see details in Gillot et al., 2006; Hildenbrand et al., 2018). The final age is obtained when individual determinations overlap within uncertainties at the 1σ level. In order to keep consistency with former datasets, we re-used the widely used constants (Garner et al., 1975; Steiger and Jäger, 1977) for age calculation.

4. Results

4.1. Submarine and sub-aerial geomorphology

Around Moorea and Tahiti, the DEM analysis (Fig. 3) reveals a complex submarine topography composed of promontories, canyons, seamounts, ridges, hummocky terrains and smooth areas. Moorea is in the middle of a rectangular area, which is limited to the north and south by two east–west trending ridges, to the west by a seamount and to the east by Tahiti. The lowest topographic point between two ridges (north and south) is about 3700 m deep (4300 m south of the southern ridge), with the submarine elevation gradually increasing from it towards Moorea and Tahiti or more steeply towards the seamount located west of Moorea.

Two massive landslides originating from Tahiti, previously described by Clouard et al. (2001) and Hildenbrand et al. (2004, 2006) are clearly identifiable. The related debris-avalanches (hummocky texture) are here highlighted in pink (Fig. 3). Two similar hummocky patterns, though much smaller, are observed to the northwest and southwest of Moorea. The sector north of Moorea is covered by less-rugged (smooth zone), massive deposits, creating a pronounced bathymetric bulge that leans against the northern ridge down to isobath −3000 m. A canyon originating from Tahiti delineates the eastern part of the bulge.

The base of the volcano (considering the −3000 m isobath around Moorea) has a drop-like shape: circular in the south and pointed in the north. In the southwest, the shoreline is concave, whereas the −3000 m isobath is convex. To a lesser extent, a similar pattern is observed on the eastern side, but with a steeper slope. The southern tip is flat to convex both at the shoreline and the −3000 m isobath. The northwestern, northeastern and northern tips are similar to the southern tip.

The subaerial shaded DEM on Fig. 3B (Moorea) highlights a horseshoe shaped crest line that opens towards the north. The outer part of this crest line consists of valleys that are more or less radial, while the inner part consists of a large topographic depression in which Mt Rotui lies. The northeastern corner of the island, appears to be poorly dissected as does a small "triangular planeze" (Fig. 3B) connected to the crests in the eastern-southeastern side.

At Tetiaroa (Fig. 3A), a distinct scar affects the island's southern flank, resulting from a collapse (Terry and Goff, 2013), likely late or a post-magmatism as nothing came to fill the gap. A topographic bulge, outlined by the −3000 m contour at the lower tip of the scar, indicates the deposition of displaced material.

4.2. New geological data

Figs. 4 to 6 summarize our main field observations, and show the location of the samples collected for dating purpose (age results in the next section). At the scale of the island, the following main volcanic units were recognized:

1. An old volcanic sequence exposed in the deepest valleys incising the southern sector. It consists of a suite of dark vesicular lava flows with weak layering showing an overall dominant external dip, i.e., roughly towards the south. Some of them are significantly weathered, and contain a high amount of zeolites, while others are slightly more massive and well-preserved (Fig. 5A). One sample from the lowermost accessible part of the succession was collected in the core of the Vaianae valley (sample MO24L, Fig. 4). Two additional samples from the same succession were collected a bit further south, closer to the outlet of the Atiha valley (samples MO22A and MO24N, respectively). Finally, one additional massive lava flow was sampled at a higher stratigraphic level in the southern wall of the central depression, along the pathway to the "Col des 3 Cocotiers" (labeled "3 Coconuts" in Fig. 4) viewpoint (sample MO22N).

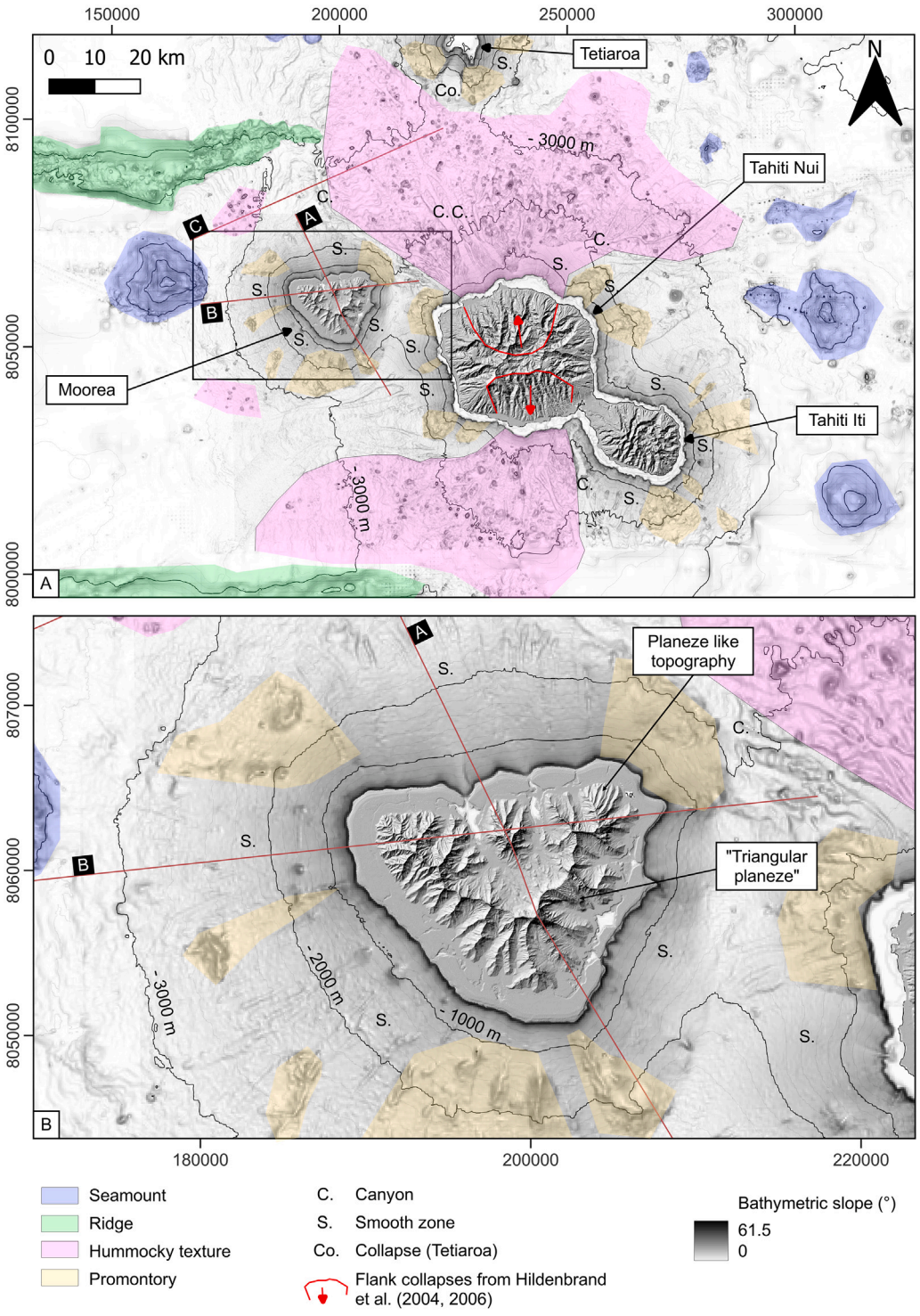

Fig. 3. DEM analysis. Aerial parts represent shaded DEM while submarine shades of gray represent the slope intensity. Submarine DEM also subtly appears as contour lines. A — Large-scale DEM analysis. Some artifacts (lines or regularly spaced dots) are visible in some parts of the map. The black rectangle refers to the close-up map shown in B. Contours are shown every 200 m (light gray line) and master contours are shown every 1000 m (black line). The black zone/contour around the emerged islands is the outer edge of the coral reef. The coordinate system around the map is EPSG:3297 (RGPF/UTM zone 6S), units are in meters. White letters on a black background and red lines refer to Fig. 7 cross sections.

2. A second main volcanic sequence dominantly represented in the northern half of Moorea (mostly N and NE sectors). Several sub-units can be distinguished:
(i) a basal monogenetic breccia made of coarse-grained scoriae deposits with peridotite nodules. This unit is exposed along the coastal road in the western part of the Paopao and Opunohu bays (Fig. 5B, C), as well as at the base of Mt Rotui southern cliff. The breccia seems to extend over part of the main depression south of Mt Rotui, but is difficult to follow due to intense weathering, erosion and extended vegetal cover. It consists of thick deposits whose visible thickness is comprised between few meters and several tens of meters. Decimetric lava flows of the same mafic

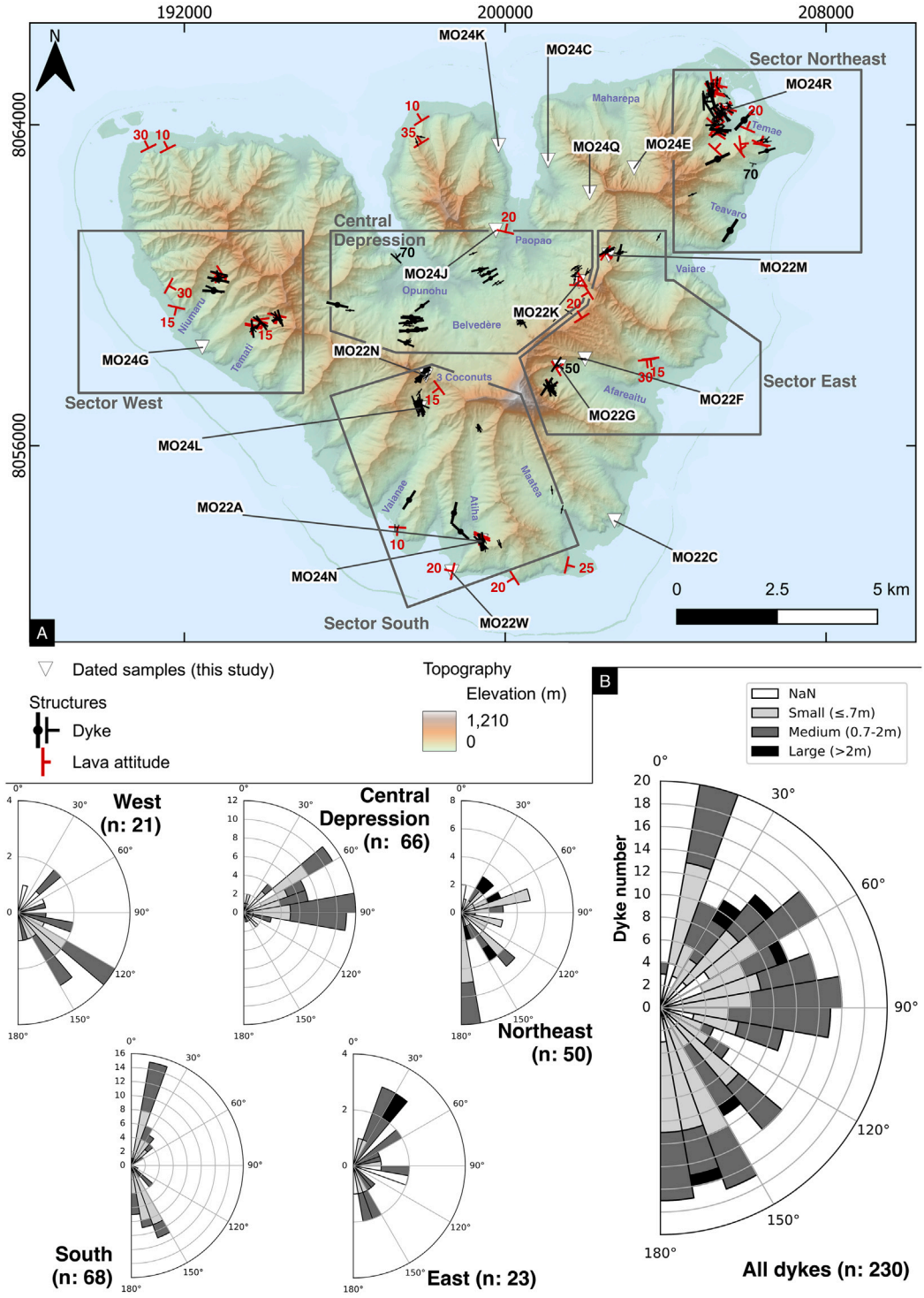

Fig. 4. A — Location and orientation of observed dykes and lava directions. For the dykes: the bigger the symbol, the thicker the dyke. Dykes with no reported size value are featured as a small dyke. We added 13°E to measured magnetic strike to account for declination. Some local names are given. B — Rose diagram (on 180°) for all dyke directions and for the northeast, east, south and west sectors circled in A. Thickness of the dykes is discriminated with shades of gray. See supplementary material S1 to picture the extension of the visited locations. NaN stands for dykes where the thickness is not reported.

composition (oceanite) may be interbedded within the breccias. Part of it being buried or covered by sediments and vegetation, its real thickness remains difficult to estimate. No specific and easily identifiable succession was observed. It shows an overall northward pronounced dip (locally > 25°) typical of proximal strombolian fallout deposit. A lava flow (MO24J) intercalated in the breccia, and a differentiated (benmoreite) lava flow covering the breccia further north (MO24K) were sampled for subsequent dating;

(ii) a thick intermediary succession of basaltic pāhoehoe or basaltic (oceanite or ankaramites) regularly spaced submetric ʻaʻā lava flows (Fig. 5D, E). Most of them are highly vesicular and pāhoehoe flows typically exhibit a complex geometry featuring lava-tubes and surficial ropes (Fig. 5D). They crop out in the

Fig. 5. Field observations. A — Vaianae deep floor (MO24L): Numerous prismatic dykes are highlighted in white in the image; a man shows the scale. B — monogenetic breccia with thin intercalated lava lenses; a standing man is included for scale. C — Peridotite enclave within a lava lens visible in B; finger for scale. D — Pahoehoe lava flows from Paveo (near MO24F), hammer for scale. E — Regular ʻaʻā lavas (oceanites and ankaramites; highlighted in white) with intercalated scoriaceous breccias (Temae sector). A 3 to 10 m wide massive dyke is crossing the sequence. F — Thick ʻaʻā basaltic lava (MO24G), 3–5 m high, with a scoriaceous base. The reddish layer at the base of the scoriaceous breccia is a paleosoil, with a hammer placed on it for scale. Beneath the paleosol lies a thick (meter-sized) ʻaʻā benmoreite flow (MO24H). G — Massive channelized benmoreite with a laminated base (MO22C); a standing man is included for scale. H — Sampling site of MO24C at a core of a highly weathered lava flow. I — Location of the picture H in the landscape. J — Temae water tank site, featuring a massive polygenetic breccia with meter-sized blocks. The overlying fence is 2 m high. K — Trachytic neck dated by Maury et al. (2000) in the landscape.

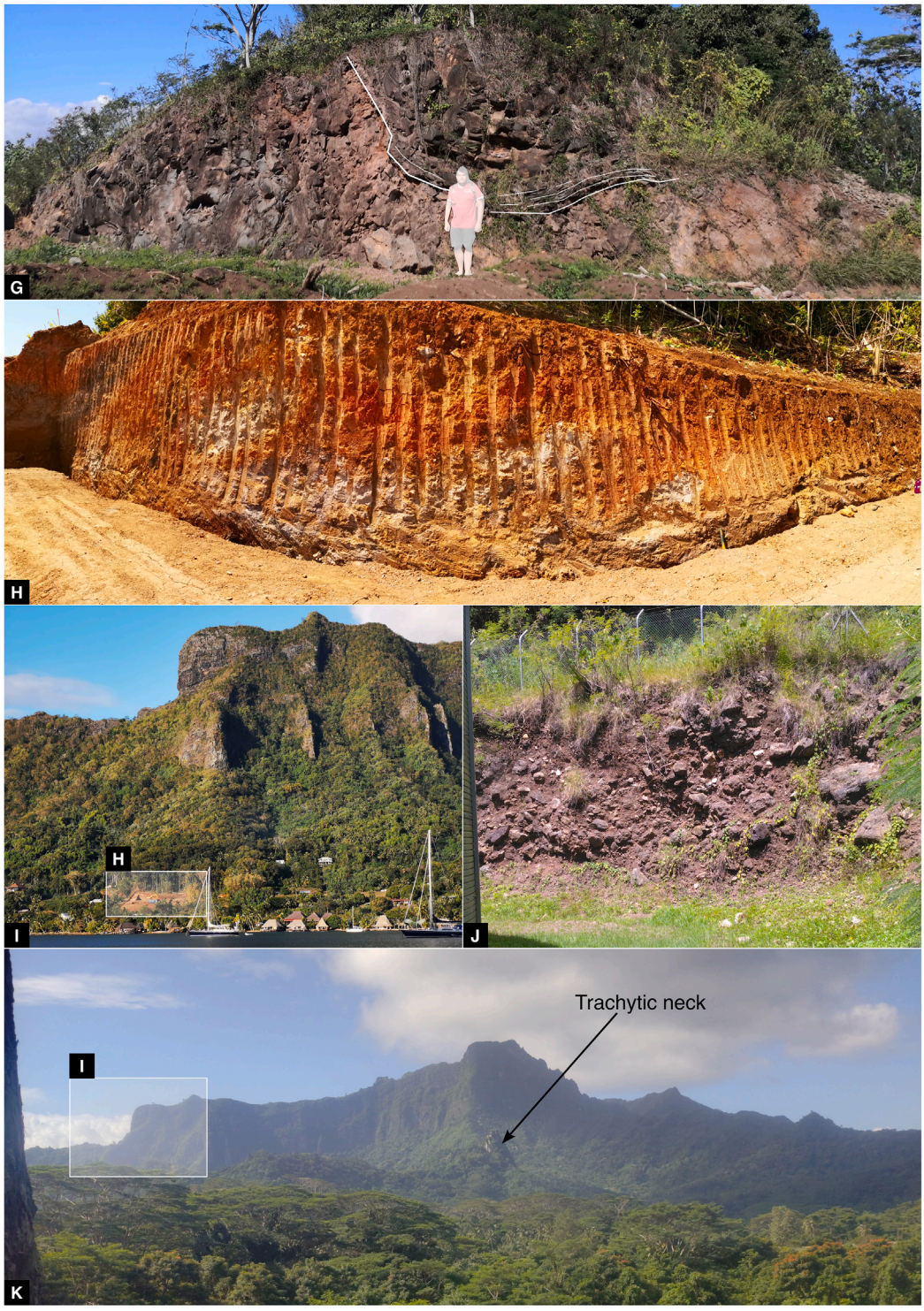

Fig. 5. (*continued*).

cliffs east of Mt Rotui, and in the northeastern and eastern sectors of the island where they show a dominant outward dip. Several of these lava flows were sampled: MO22N, MO24Q, MO24E and MO24R;

(iii) A suite of massive, plurimetric and generally prismatic, mafic to evolved lava flows (Fig. 5F, G). These generally constitute the upper parts of the main summits in the northern and eastern part of Moorea, previously dated around 1.55–1.52 Ma (Le Dez et al., 1998; Guillou et al., 2005). Similar lava flows also crop out along the southern and western coasts (MO22C, MO22W, MO24G). There, they clearly show a channeled geometry (Fig. 5F, G), suggesting late filling of (paleo-) valleys at the time of eruption.

3. Other recent volcanic units include subsidiary flows and necks encountered mostly in the northern depression. With rift zones spotted in the central depression, they generally constitute second order hills that can be spotted on the DEM (Fig. 4). We especially sampled a thick columnar basaltic lava flow (sample

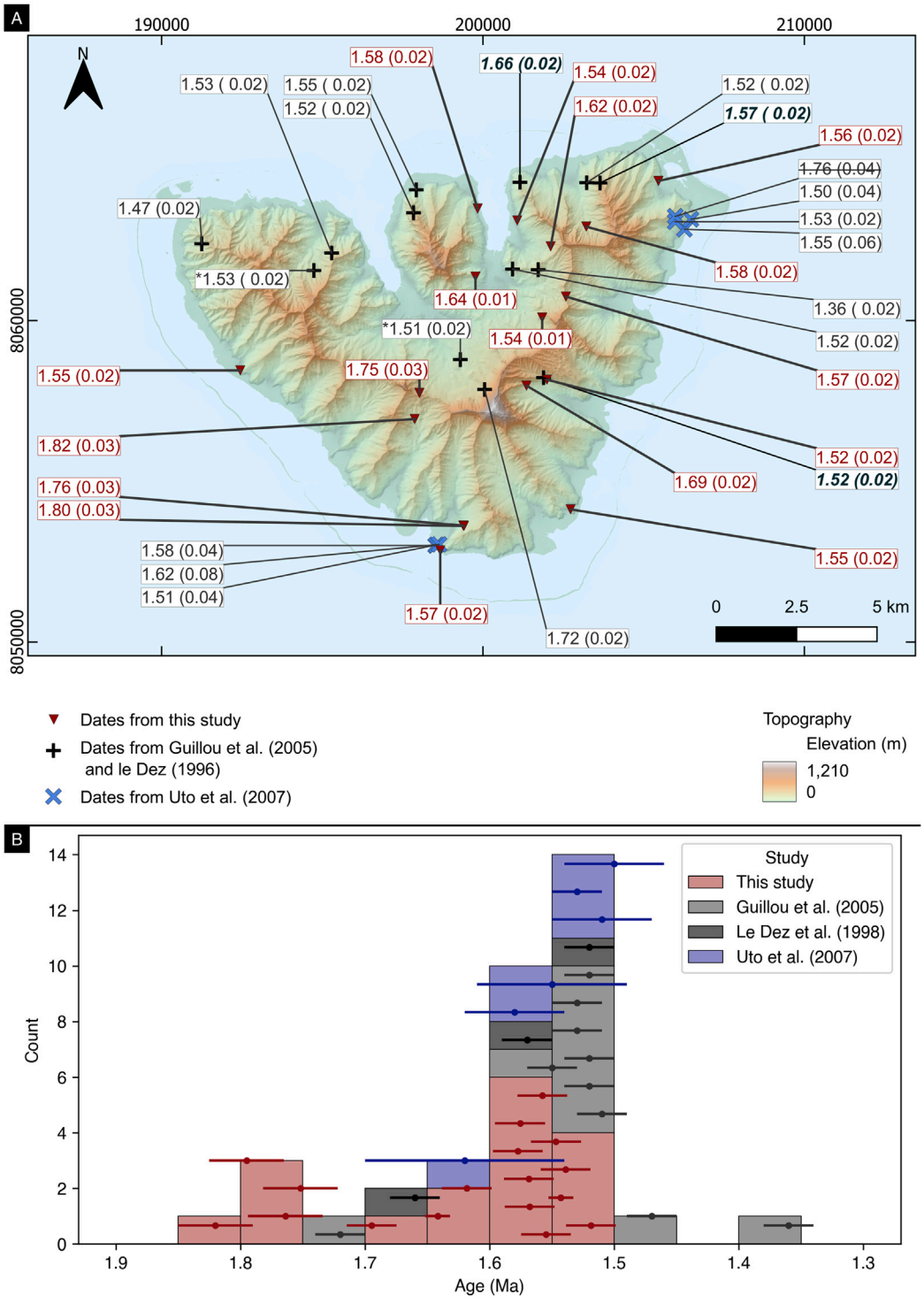

Fig. 6. A — New K/Ar ages (in Ma) on fresh separated volcanic groundmass (red color). Previous ages from Le Dez (1996), Guillou et al. (2005) and Uto et al. (2007) are shown in black. B — Age histogram of the dated rocks of Moorea. Individual age determinations and their uncertainties ($\pm 1\sigma$) are shown with dots and horizontal bars, respectively. Le Dez et al. (1998) refers to the 3 dates in bold letter from Fig. 2 or in Fig. 6A.

MO22K) with a local southwestward dip that was apparently erupted from a strombolian cone at the foot of the main depression wall (Fig. 4). The fresh core of a highly weathered lava flow with an apparent northern dip (MO24C; Fig. 5H, I) was also collected at the base of a low-relief along the eastern side of the Opunohu bay. This relatively low-relief may either represent the distal part of a late valley-filling flow, or alternatively an older unit exposed by recent incision at the base of the main cliff. Finally, the young trachytic neck of Paopao (Fig. 5K), and the young benmoreitic sequence of Papetoai emplaced along the NW side of the main depression were not sampled here, as they had already been extensively investigated and dated in previous works (Le Dez et al., 1998; Maury et al., 2000; Guillou et al., 2005).

Polygenetic epiclastic breccias (Fig. 5J) are widely exposed across the island, predominantly along valley slopes and in riverbeds. They generally occur as dark brownish more or less indurated layers comprising poorly sorted angular to sub-rounded decimetric volcaniclastic lava blocks cemented by a clayey matrix. Like in Tahiti where similar deposits were observed (Hildenbrand et al., 2008), these breccias may either represent indurated talus, mudflow or debris flow deposits that experienced late cementation and/or induration in the presence of water (see also Bret et al., 2003). These polygenetic breccias thus most likely accumulated predominantly in valleys/canyons as a result of erosion processes, and will be referred to as "torrential breccias" for the remainder of this paper. In Moorea, most of these deposits cover the various volcanic units and are thus recent. A few of them, however, seem intercalated with volcanic products. This is the case in the Afareaitu valley, where torrential breccias have been attributed to the oldest geological units of the island (Maury et al., 2000). In the deepest part of the valley (western waterfall), we sampled (1) a dark lava (sample MO22G) covered by torrential breccia layers, and (2) a massive basaltic lava flow (MO22F) from the younger volcanic sequence overlying them.

A total of 230 dykes was located in this study (Figs. 4, 5A, E). Most of them are prismatic, sub-vertical and less than 2m-thick. They do not seem equally neither radially distributed, but instead occur as swarms with preferential orientations. A main E–W swarm was recognized in the SW part of the central depression, and extends to the western sector (Niumaru valley). This swarm direction (ranging from N50°E to N110°E) represents a total number of 84 dykes of the island, which corresponds to 36.5% of the total amount of measured dykes. In the inner parts of the southern valleys, the oldest volcanic units are cut by numerous dykes trending either NNE (N15°E) or SSE (N155°E). The latter direction is also represented in the western sector within the headwall of the Temati valley. In the eastern sector, including the eastern part of the central depression and the Afareaitu valley, the dominant orientation shifts to the northeast (N55°E). Finally, in the northeastern sector, dyke orientations are more variable, with a dominant N–S trend (N175°E), accompanied by secondary directions towards the ENE (N75°E) and SE (N135°E).

4.3. New K/Ar ages

The new K/Ar ages obtained in this study range between 1.82 ± 0.03 Ma and 1.52 ± 0.02 Ma (Table 1, Fig. 6). They are generally consistent with previous K/Ar determinations on separated groundmass obtained for samples collected on similar units where applicable (Le Dez et al., 1998; Guillou et al., 2005; Uto et al., 2007). Furthermore, our new geochronological data on the three main volcanic sequences newly recognized here are mutually consistent and fully match the available stratigraphic control.

The volcanic sequence exposed in the southern sector is newly dated between 1.82 ± 0.03 Ma (sample MO24L) and 1.75 ± 0.03 Ma (MO22N), and possibly, up to 1.69 ± 0.02 Ma from the age obtained our sample MO22G underneath the torrential breccias in the Afareaitu valley. Notably, the two determinations obtained on distinct fractions of the separated groundmass for our oldest sample MO24L overlap at the 1σ level, testifying that the sample has not suffered any significant internal disturbance, ruling out any potential effect of weathering and/or zeolitization. The obtained age of 1.82 ± 0.03 Ma is thus robust and brings an important new maximal temporal bound for Moorea early volcanic activity. Other ages of 1.76 ± 0.03 Ma (sample MO22A) and 1.80 ± 0.03 Ma (MO24N) obtained on the two distinct lava flows collected close to each other in the Atiha valley are mutually consistent and very similar to the oldest age, overall reinforcing robust volcanic activity around 1.80 Ma. Finally, the age of 1.75 ± 0.02 Ma obtained on the lava flow collected in the upper part of the succession within the main wall of the northern depression is logically younger, and comparable with the age of 1.72 ± 0.02 Ma obtained by Le Dez et al. (1998) on a sample collected at a similar level farther east (Figs. 4 and 5). Although the discarded date from Uto et al. (2007) is consistent with our new ages (1.76 ± 0.04 Ma), it was disregarded by the authors for methodological reasons and will not be addressed further in this article.

The new ages here measured on the second main volcanic sequence exposed on the northern half of the island range between 1.64 ± 0.01 Ma and 1.52 ± 0.02 Ma. The highest value is obtained on the lowermost lava flow intercalated in the strombolian deposits at the base of the Mt Rotui southern cliff (sample MO24J). Independent measurements on the two density fractions of this peculiar sample yield strictly similar age results, despite variable initial K-content. This provides a well-resolved temporal constraint, and rules out any doubt about a potential age bias, e.g., due to the incorporation of inherited excess-argon, showing that any potential peridotite micro-xenolith were effectively removed during the separation process. The new ages obtained on samples collected farther north (evolved lava MO24K) and on the side of the intermediary pāhoehoe lava succession exposed east of Mt Rotui (samples MO24Q and MO24E) range between 1.62 ± 0.02 Ma and 1.58 ± 0.02 Ma. The oldest of these is compatible within uncertainties with a previous age of 1.66 ± 0.02 Ma by Le Dez et al. (1998) (Fig. 2). The latter age, however, was obtained on a sample located at relatively high altitude, and the age was later discarded by the authors. Notably, our new ages on lava flow samples collected on the outer island flank in the eastern and northeastern sectors (samples MO22M and MO24R) yield ages of 1.57 ± 0.02 Ma and 1.56 ± 0.02 Ma, overall pointing to a robust phase of volcanic construction throughout the northern half of Moorea at this epoch.

Finally, the late prismatic, often valley-filling, basaltic to benmoreitic lava flows exposed in the various sectors of Moorea are here extensively dated between 1.57 ± 0.02 Ma (MO22W) and 1.52 ± 0.02 Ma (MO22F). The youngest age is strictly similar to a previous age of 1.52 ± 0.02 Ma obtained by Le Dez et al. (1998) on a lava flow collected at a similar level in the same succession (upper Afareaitu valley wall).

5. Discussion

5.1. Comparison with previous studies

This study confirms some of the conclusions from previous works, but also draws major differences regarding the geological knowledge of the island.

Our new data show that the geological map (Fig. 2, Maury et al., 2000) requires significant update and revision: (1) the oldest units reported on the geological map consist of laharic breccia layers such as the ones observed in the Afareaitu valley; instead, we here show that these breccia are younger than 1.69 ± 0.01 Ma, and thus do not constitute the oldest formations at the surface of the island; considering the new ages here obtained, these breccias most likely accumulated in a small paleo-valley after a late volcanic episode ending the first shield building-phase; (2) similar "old" breccia units mapped in the other valleys may in fact represent recent torrential breccias, as they cover most volcanic units, including recent volcanic units; this is the case in the north, where 'old breccias' on the map are covering the recent volcanic sequence of Mt Rotui; (3) volcanic successions in the northern and southern sides of the island were mapped as the products of one single main shield edifice. We here show that the deepest valleys in the southern part of the island incise the preserved flank of an old volcanic edifice here dated between ca 1.85 and ca 1.70 Ma, while all the geological units exposed in northern Moorea, even the most basal one, are younger than 1.66 Ma. It has important implications regarding the architecture and the evolution of the island, as the northern depression cannot result from a recent collapse process that affected a symmetrical volcanic edifice; instead, it underlines a major contact between two nested successive volcanoes of different ages; (4) the use of recent open-source bathymetric data improves the understanding of the submarine volcanic structure, revealing a distinct bulge north

Table 1
New K/Ar results on fresh separated groundmass. The mean age is obtained by weighting the amount of radiogenic argon (^{40}Ar*), except in the case of samples MO22C and MO22K, for which more than 2 independent argon analyses have been achieved; for the latter, the mean age is calculated by weighting by the inverse of variance. Measured ages in normal font, and mean ages in bold font. Uncertainties quoted at the 1σ level.

Sample	Long	Lat	K (%)	^{40}Ar* (%)	^{40}Ar* (10^{12} at/g)	Age (Ma)	1σ
MO22A	−149.83211	−17.58374	1.348	47.55	2.492	1.770	0.025
				51.14	2.477	1.759	0.025
					Mean :	**1.764**	**0.025**
MO22C	−149.80061	−17.57965	4.305	63.77	7.015	1.559	0.022
				75.46	6.992	1.554	0.022
				74.38	6.975	1.550	0.022
					Mean :	**1.555**	**0.013**
MO22F	−149.80697	−17.54313	0.480	14.33	0.767	1.530	0.024
				19.32	0.757	1.510	0.023
					Mean :	**1.519**	**0.023**
MO22G	−149.81299	−17.54473	2.334	50.71	4.147	1.700	0.024
				42.61	4.116	1.688	0.024
					Mean :	**1.695**	**0.024**
MO22K	−149.80809	−17.52572	1.315	21.99	2.103	1.530	0.023
				21.01	2.156	1.568	0.023
				23.02	2.105	1.532	0.023
					Mean :	**1.543**	**0.013**
MO22M	−149.80106	−17.51988	1.452	26.55	2.366	1.559	0.023
				26.42	2.393	1.577	0.023
					Mean :	**1.568**	**0.023**
MO22N	−149.84437	−17.54633	1.230	31.27	2.245	1.747	0.025
				22.33	2.259	1.758	0.026
					Mean :	**1.752**	**0.026**
MO22W	−149.83896	−17.59064	1.312	34.26	2.148	1.567	0.023
				34.29	2.152	1.570	0.023
					Mean :	**1.568**	**0.023**
MO24C	−149.81497	−17.49829	1.960	16.94	3.135	1.531	0.023
				16.44	3.168	1.547	0.024
					Mean :	**1.539**	**0.024**
MO24E	−149.79478	−17.50032	1.426	36.14	2.342	1.572	0.023
MO24Ebis			1.381	37.17	2.284	1.583	0.023
					Mean :	**1.577**	**0.023**
MO24G	−149.89673	−17.53923	1.669	26.25	2.695	1.545	0.023
				43.12	2.698	1.548	0.022
					Mean :	**1.547**	**0.022**
MO24J	−149.82745	−17.51391	1.225	42.06	2.084	1.628	0.023
				42.74	2.123	1.659	0.024
MO24Jbis			1.298	37.76	2.234	1.647	0.024
				38.88	2.216	1.634	0.023
					Mean :	**1.642**	**0.012**
MO24K	−149.82652	−17.49481	4.314	53.52	7.097	1.574	0.022
				57.71	7.107	1.577	0.022
					Mean :	**1.576**	**0.022**
MO24L	−149.84587	−17.55363	0.965	38.23	1.811	1.797	0.026
MO24Lbis			1.016	35.28	1.959	1.845	0.027
					Mean :	**1.820**	**0.026**
MO24N	−149.83192	−17.58385	1.245	40.05	2.333	1.794	0.026
				36.90	2.337	1.797	0.026
					Mean :	**1.795**	**0.026**
MO24Q	−149.80530	−17.50572	1.461	23.90	2.453	1.607	0.024
				16.69	2.496	1.635	0.025
					Mean :	**1.618**	**0.024**
MO24R	−149.77347	−17.48780	1.402	27.79	2.284	1.559	0.023
				47.01	2.281	1.557	0.022
					Mean :	**1.558**	**0.022**

of the island, which brings important new information to explain the topographic and geological strong asymmetry of the island (Fig. 3). A more robust model for the building stages of Moorea has yet to be proposed.

5.2. Proposal of a new model of evolution

The first-order geometric relationships between the main geological units here recognized and dated have been first reported on two cross-sections at the island scale (Fig. 7). These serve as a basis to discuss the extent and the timing of the main successive steps of construction and destruction of the island. The objective here is to provide temporal and structural constraints on the island's key stages of evolution.

5.2.1. A Somma from a first volcano

The remnants of the older edifice (Figs. 7 and 8, panel 1, sh1) here dated between 1.82 ± 0.03 Ma and 1.72 ± 0.03 Ma crop out in the southern part of the island up to a maximal elevation of about 400 m at the "three coconut trees" passage. Strikingly, these old lavas generally dip towards the south, while no counterparts dipping to the north are observed at the surface, despite the presence of the deep central topographic depression. In the hypothesis of an initial symmetric volcanic edifice, a significant portion of the former northern flank is missing at the surface. The exact position of the main eruptive center cannot be retrieved precisely, but it may have been located near the Belvédère (upper Opunohu valley) from the presence of many dykes

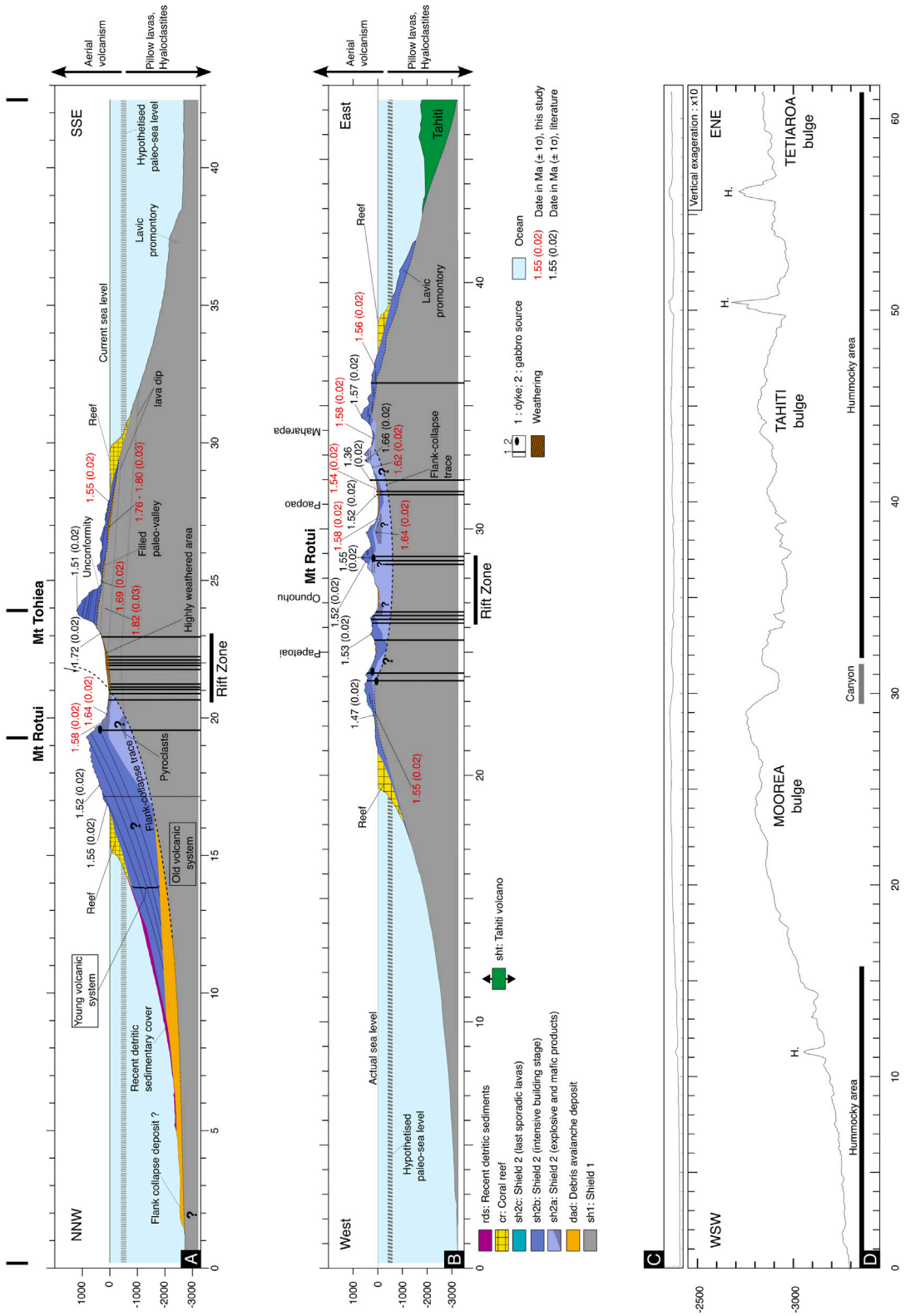

Fig. 7. Cross-sections from Fig. 3 illustrating observations and ages in Ma (±1σ). Ages in red are from this paper, other are from Le Dez et al. (1998) and Guillou et al. (2005). A — NNW–SSE summary cross-section (no vertical exaggeration) depicting the proposed structure of a northern landslide. The black thick vertical line above cross section A represents minor inflexion nodes in the cross section on Mt Rotui and Mt Tohiea. Reef thickness and former sea-level are indicative. The subsidence from Fadil et al. (2011) and Thomas et al. (2012) is assumed constant. The light blue area represents the rocks resulting from the decompressive response and the subsequent lavas that followed the flank collapse (pyroclasts and highly mafic pāhoehoe lavas). Dark blue stands for the following eruptive products. B — W–E summary cross-section (no vertical exaggeration) showing another perspective of the northern landslide structure. Note the presence of Tahiti-derived deposits in the submarine eastern portion of the section, as well as the steeper slope of the eastern flank. C — (no vertical exaggeration) and D — (vertical exaggeration x10) emphasize the bulge visible in the bathymetric data north of Moorea. 'H.' denote hummocks located directly on the cross-section. Abscissa values are in km, ordinate ones are in meters relatively to the sea level.

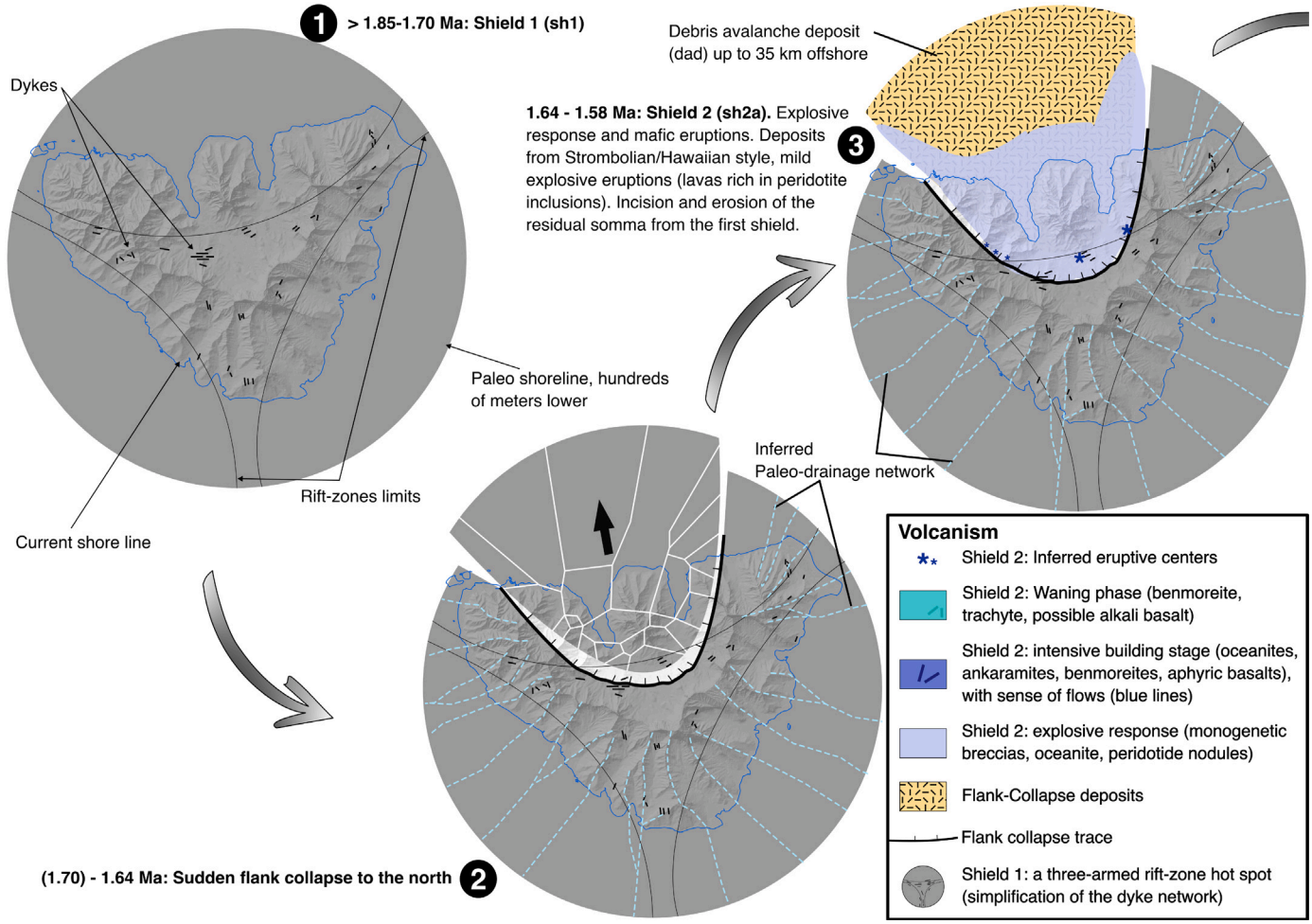

Fig. 8. Schematic model of edification of Moorea volcano featuring a three-armed rift-zone hot spot (Shield 1) affected by a northern flank collapse. The construction of a second shield and recent detritic sediments have partly obliterated the first one that is only accessible in the south.

in this sector (Fig. 5B). Parts of the old volcano flanks may also be presently hidden under recent volcanic units, especially in the NE and NW sectors.

Our new ages show that the older rocks were overall emplaced during the Olduvaï normal magnetic polarity (Uto et al., 2007; Singer, 2014; Ogg, 2020) while, until now, it was believed that the island had fully emplaced during the subsequent reverse magnetic polarity. Therefore, the search for relicts of the old volcano at depth may be conducted through geophysical investigations (e.g., magnetic surveys) in the future (e.g.: Dumont et al., 2021).

5.2.2. A northern flank collapse

Several processes may explain why the old edifice northern flank is presently lacking at the surface: (1) downward movement along an E–W normal fault, which would have gradually offset nearly half of the former volcano, before (or during) the second volcanic stage (1.64 Ma–1.35 Ma). This appears rather unplausible, because no major fault trace seems to cut the submarine parts of the island and flatter dipping lavas should be observed on the northern side of Mt Rotui instead of the observed dips as high as 30 to 40°N; (2) erosion of the full northern part of the island, before construction of the second main volcanic sequence. Such hypothesis also seems unlikely, as it would require complete removal of a huge amount of volcanic material within only a few tens of thousand years; furthermore, incision by regular erosion would most probably have left obvious morphological relicts; (3) A northern flank collapse. Although no debris avalanche deposits (dad) were observed on the field, this hypothesis is our preferred one (Figs. 7 and 8, panel 2) as it is supported by (i) the presence of large blocks up to 30 km offshore north-northwest of Moorea (Figs. 3 and 7C,D; dad), which are here interpreted as the distal parts of fast-running debris-avalanche deposit, and (ii) extended strombolian deposits (sh2a, explosive) including peridotite nodules at the base of Mt Rotui (Fig. 5); these support a major episode of decompression of the magma-feeding system (Fig. 8, panel 3), which we attribute to immediate eruptive response to the collapse, as proposed for many other oceanic islands (Hildenbrand et al., 2003, 2004, 2018, 2024; Quidelleur et al., 2008; Manconi et al., 2009; Boulesteix et al., 2012, 2013; Costa et al., 2015; Marques et al., 2025). On Moorea, the new age of 1.64 ± 0.01 Ma obtained on the base of the post-collapse volcanic sequence is our best estimate for the timing of the inferred flank collapse (see also discussion in Quidelleur et al., 2008). The geographical extent of the collapse is delicate to constrain due to recent volcanism and erosion. From the observed bathymetric features in the northern area (Fig. 3), it may coincide with the smooth area between the two bathymetric promontories. This area also shows two inflection points in the coral reef system, possibly highlighting the trace of the flank collapse structure, as observed for the giant northern and southern landslides in Tahiti Island (Hildenbrand et al., 2006).

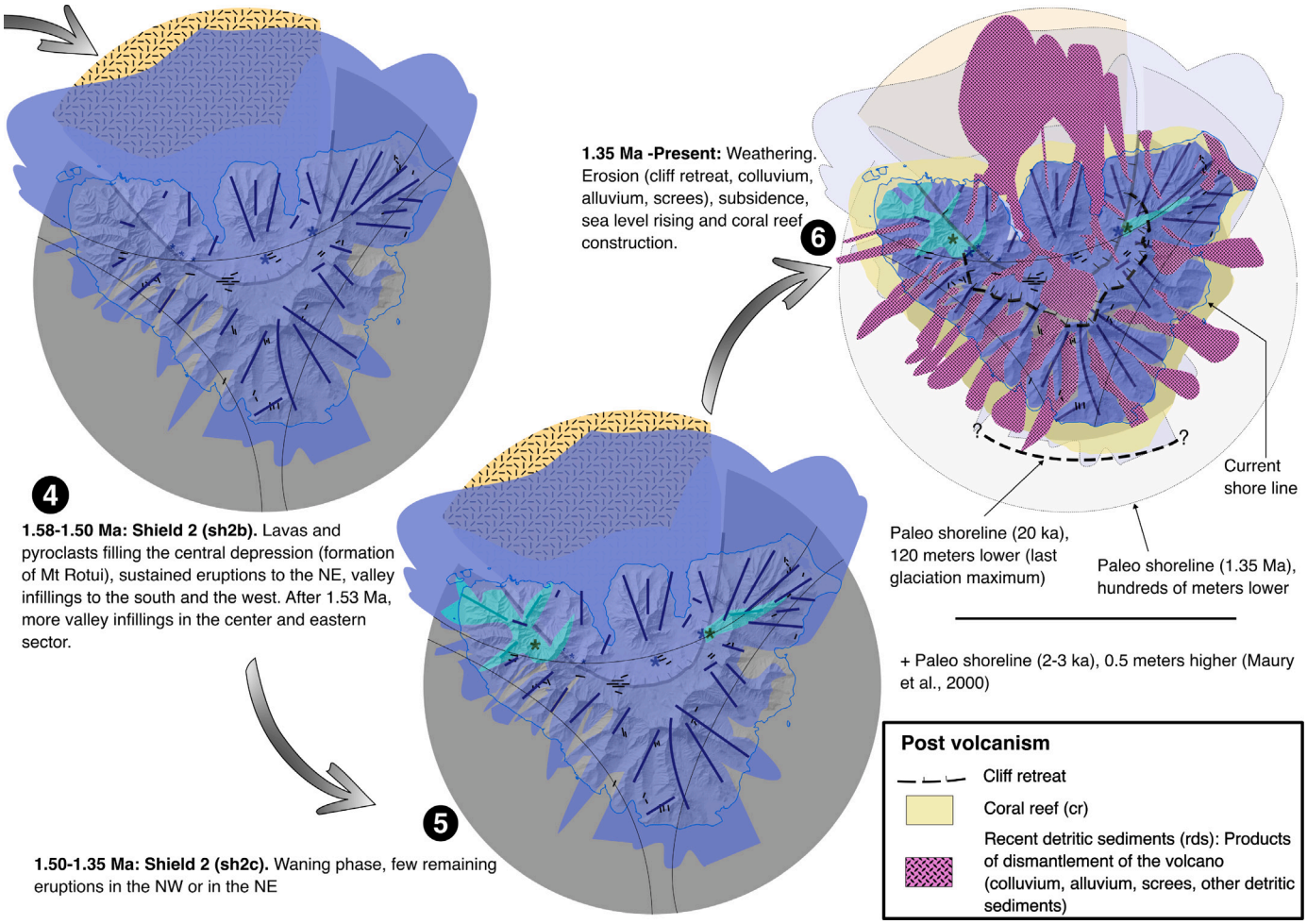

Fig. 8. (*continued*).

5.2.3. Filling the landslide depression and planeze building

The northern flank collapse was followed by vigorous volcanic activity between at least 1.64 ± 0.01 Ma and 1.58 ± 0.02 Ma (Figs. 7 and 8, panel 3, sh2a). The age of 1.66 ± 0.02 Ma obtained by Maury et al. (2000) on a lava sample in the Paveo area (Fig. 2) is consistent with such a scenario, although it was apparently collected at a relatively high elevation around 170 m. Alternatively, it may represent a collapsed block from the old volcanic edifice that was not fully evacuated by the landslide (Toreva block), as observed for the landslide associated with the 1980 eruption of Mount St Helens (Siebert and Reid, 2023), and/or in analog experiments (Oehler et al., 2005).

In any case, available geochronological data support initial rapid construction of at least one volcanic edifice within the landslide depression. Throughout this phase, the old volcanic shield was progressively incised, leading to the development of significant valleys in the southern sector, and most probably also in the northwestern and northeastern portions bounding the slide depression. Although not systematically observed, polygenetic breccias intercalated between the old volcanic basement and more recent lava flows are likely present, buried beneath the latter.

Around 1.58–1.56 Ma, basaltic to benmoreitic eruptions (sh2b), including pāhoehoe and submetric regular ʻaʻā lavas, reached the island outer flanks, leading to significant re-surfacing. The volcanic sequence in the NE area was probably erupted from vents located further to the SW, e.g., in the south-eastern part of Paopao sector (Figs. 4 and 6). It may correspond to the Bouguer anomaly identified by Shih et al. (2015) around Mt Mouaputa. Given the substantial lava deposit (>200 m thick) and the regularity of the flows observed in Temae and Perehue (a small valley, directly north of Temae valley where an old pluri-decametric quarry wall shows the superposition of metric to sub-metric ʻaʻā flows), we infer that it was fed by a significant eruptive center. Another lava flow was observed north of Mt Mouaputa, flowing eastward. It was likely emitted from the same eruptive center.

The benmoreite lava flow erupted at the same time further to the west (sample MO24K, here dated at 1.58 ± 0.02 Ma) may originate from the central vent that formed Mt. Rotui, as it overlies some monogenetic breccias. The evolved character of this lava points to partial connection with a shallow magma reservoir in this area, which is overall consistent with the presence of coarse-grained rocks in the area (Nepheline and biotite bearing gabbros, Deneufbourg, 1962).

5.2.4. Filling up paleovalleys: overflowing or multiple dispersed eruptive centers?

Between 1.58 and ca 1.50 Ma, many lava flows were erupted across the island (Fig. 8, panel 4 and 5; sh2b). In the northern part, the upper part of the Mt Rotui records late basaltic to benmoreitic effusions activity dated between 1.55 ± 0.02 Ma and ca 1.52 ± 0.02 Ma (Le Dez et al., 1998). This sequence supports continuing eruptions from a main edifice further growing within the main northern landslide depression, atop a shallow magma reservoir. In the meantime, lava flows erupted within the southeastern end of the main depression support an existing parasitic cone developed at the foot of the main collapse scar, 1.54 ± 0.01 Ma ago (sample MO22K). The age of 1.54 ± 0.02 Ma additionally obtained on our sample MO24C in the lower part of the

Opunohu valley is strictly similar, and supports late valley-filling by lava erupted from the similar vent.

During the same period, basaltic to benmoreitic lava flows eruptions reached the southern sector, filling a paleo-thalweg or valleys, e.g., south of Atiha valley (Figs. 4 to 6). The channeled geometry of several lava flows here dated between 1.55 ± 0.01 Ma (sample MO22C) and 1.52 ± 0.02 Ma (MO22F) indicates that the old volcanic shield had undergone incisions in various locations, as confirmed by the "old" torrential breccias in the Afareaitu valley (see MO22F, Fig. 4). From the contact between the old and recent volcanic series, and available morphological evidence, several of these flows were most likely erupted from parasitic cones developed on the eroded slopes of the old volcano.

Finally, volcanic activity decreased (sh2c) due to relative eastward displacement of the hotspot (to Tahiti Nui). Recent rocks, dated by Maury et al. (2000) are benmoreites (1.47 Ma in Papetoai) or trachyphonolite in the center of the Paopao valley (1.36 Ma). As the fusion rate decreased, alkali basalt could also be expected.

5.2.5. Post-volcanic landscape evolution

Following the cessation of volcanic activity, the island has undergone extensive modification (Fig. 8, panel 6) due to subsidence, the coral reef (cr) building in the last thousands of years (Maury et al., 2000) or through both physical (recent detritic sediment: rds) and chemical erosion. Understanding the full impact of these processes remains one of the most challenging and unresolved questions to date. As a first order hypothesis, it is reasonable to suggest that the more resistant and permeable nature of recent lava flows has contributed to topographic inversions. While this explains the morphology of the southern valleys, it is less satisfactory for the northern part of the island, where significant amounts of younger lava have been observed.

In the central region of the island, the structural fabric of the volcano has likely influenced erosion patterns (Jefferson et al., 2014). The flank collapse scars and their associated overlying breccias may have formed an impermeable barrier that guided the pathways of underground water. The numerous associated dykes may also have acted as preferential pathways for water diffusion and/or water circulation, as evidenced on Tahiti (Hildenbrand et al., 2005, 2008) or as impermeable barrier impounding the water tables and segmenting the existing aquifers (Izquierdo, 2014; Marazuela et al., 2023). We also cannot exclude the effect of edifice geometry on water streamflow due to the general northward dip of the post-collapse succession, with an initial angle locally exceeding 20° (scoria cone). The study of other oceanic islands like La Palma (Canary) has shown that deep erosion can enlarge initial flank collapse structures and incise much of the post-collapse volcanic units (e.g.: Navarro and Coello, 1993; Carracedo et al., 1999; Hildenbrand et al., 2003).

Jefferson et al. (2014) suggest that subsurface chemical erosion may be the primary mechanism by which young volcanic edifices lose mass towards the ocean. The reason for this lies in the permeability of the young volcanic rocks, which inhibits the stream formation and limits physical erosion. Over time, the progressive leaching of soluble chemicals and the recrystallization of secondary minerals increase the impermeability of the subsurface, triggering physical erosion. The more impermeable the subsurface, the greater the physical erosion, the latter can account for up to 90% of total mass loss (Jefferson et al., 2014). This likely contributed to the formation of major river systems, which led to intense mechanical erosion and the development of two major valleys: Opunohu and Paopao. Aside from periodic cliff collapses that rejuvenate their surfaces (Kirch et al., 2023), the soils within these two valleys are highly ferrallitic compared to the rest of the island (Jamet, 2000). The widespread occurrence of such weathering profiles raises questions about their origins and formation timeline. Our study suggests that soil depletion is largely independent of the protolith's age. For instance, the lava flow sample MO24C shows extensive weathering at the surface, despite being one of the youngest dated in this work. This is consistent with recent works on weathering dynamics in the Azores, which showed that weathering rates under warm and wet sub-tropical (paleo-)climate is controlled primarily by the texture of volcanic units rather than by their age (Hevia-Cruz et al., 2024a,b, 2025; Loiodice et al., 2025). Specifically, fine-grained volcanic rocks, such as pyroclastic deposits and porous/permeable rocks, have a greater surface area when they come into contact with aqueous solutions. This enhances ion exchange and weathering. After rapid weathering, the rocks reach equilibrium through sufficient recrystallization of clay minerals, which inhibits water circulation within the rock. Therefore, the age of a rock is not necessarily correlated with its weathering rate.

5.3. Link between rift zones and collapse(s)?

In Tahiti, Hildenbrand et al. (2004) have shown the major influence of an E–W main rift zone, that served as the dominant feeding system and was responsible for the two opposite major landslides of the northern and southern island flanks. Subsidiary rift-zones were additionally recognized, and may be partly related to reactivation of basement discontinuities during unloading by the collapses. The main E–W direction is also marked by the development of linear submarine volcanic ridges in the region, including a main one here identified north of Moorea (Fig. 3).

Significant amounts of dykes trending E–W have also been measured here in Moorea. Interestingly, in Fig. 8, the rough alignment of the proposed main vent systems (central, NE, and NW) may also represent the E–W direction. This suggests that the alignment of the three discussed main volcanic vents along an E–W axis could have influenced the overall orientation of Moorea's northern shoreline. Another major dyke orientation in Moorea appears to be around N160°E, which aligns with the direction of the ancient ridge seafloor fabric (Hildenbrand et al., 2004, and included references). A third significant dyke orientation is here also measured approximately N25°E, while the remaining dykes exhibit scattered orientations. Altogether, the main dyke directions seem to define a triple-armed rift-zones as described elsewhere, e.g. in El Hierro and Tenerife in the Canary archipelago (e.g.: Walter and Troll, 2003; Becerril et al., 2015). As for these conspicuous examples, Moorea also shows a somewhat triangular shape in plan-view, which may partly result from forceful magma concentration along the three main directions, potentially favoring destabilization of the island slopes.

Our study of the bathymetric data (Figs. 3 and 7) suggests the presence of a northern flank collapse. At this stage, it remains uncertain whether Moorea has experienced (an)other comparable flank collapse(s). The southwestern hummocky terrain appears to be disconnected from Tahiti's landslide deposits and lies at the western limit of the highest resolution bathymetric data, preventing further investigations. It is notable that a discernible horseshoe-shaped feature follows one of the island's western crests. Similarly, the eastern side of Moorea has submarine steep slopes and a comparable horseshoe-shaped structure in its topography. However, any potential landslide deposits in this area would likely be buried beneath materials from Tahiti. Increasing the density of dated samples in these regions or enhancing the bathymetric resolution between Moorea and Maiao could help determine the validity of these hypothetical structures.

5.4. Broader implications and perspectives

Our study confirms that relatively small intra-plate oceanic volcanoes like Moorea can experience hazardous flank collapses during their lifetime. While flank failures on volcanic islands of comparable size (current emerged area around 134 km^2) have been increasingly documented worldwide (e.g., Hildenbrand et al., 2018, 2024; Sibrant et al., 2015a; Marques et al., 2019, 2025; Niyazi et al., 2025), many other cases remain unclear. For instance, several small volcanic islands in the Pacific, e.g., in the Marquesas and Samoa archipelagoes (Maury et al., 2014; Németh and Gravis, 2022; Németh and Zakharovskyi, 2025) show intriguing elongated shape seemingly truncated by arcuate scars

that may underpin past episodes of catastrophic lateral collapse. Nevertheless, our study demonstrates that geomorphological identification of old destabilization events remains challenging, as potentially-related submarine debris-avalanche deposits and their sub-aerial counterparts can be extensively obscured by subsequent volcanic and sedimentary processes. However, our methodology, combining detailed geomorphological, geological and geochronological analyses, unveil asymmetrical imbrication of nested volcanic successions even when tropical climate has greatly modified the former landscape. Understanding and identifying such structures has direct implications for fresh water exploration and its management and may, in a lesser extent, affect land use, archeological prospections, natural/industrial risk management (landslide, pollution, ...). Our methodology developed on Moorea thus constitutes a promising line of research on other small volcanic islands worldwide.

The limited understanding of such volcanic islands is largely due to the complexity of the research required, which involves field observations in challenging environments, extensive and expensive laboratory analyses. The incorporation of island-scale geophysical data, such as airborne electromagnetic survey (e.g.: Dumont et al., 2021), could facilitate the identification of paleostructures and weathering surfaces. However, the high cost of these methods often exceeds the financial resources of small island communities. In Moorea, the rock ages are straddling on a paleomagnetic inversion, which should be taken into account for future magnetic studies. The development of semi-airborne or drone-based geophysical solutions (e.g.: Arrué et al., 2024) offers a promising alternative that, once fully developed, could help to bridge this gap. Similarly, fieldwork in Moorea has at times been hampered by the inability to closely examine the extensive high cliff surfaces that can only be observed from a distance. Recent advances in hyperspectral imaging, whether ground-based (Son et al., 2022) or airborne (Miller et al., 2020), may provide a valuable tool for future investigations. In addition to their geological significance, these geophysical and volcano-structural studies could also provide critical data for hydrogeological research as in other basaltic islands (Lachassagne et al., 2014) or in other volcanic context (Toulier et al., 2019; Baud et al., 2024). With increasing concerns about water resources due to climate change and direct anthropogenic impacts, such studies will become increasingly important for sustainable resource management.

6. Conclusions

Based on the pre-existing studies, new field observations, original datings and benefiting from 20 to 60 years of volcanological and bathymetric advances, our work evidences a way to highlight the presence or absence of a moderate flank collapse in small eroded volcanic islands. Our investigations provide a better understanding of the structural complexity and history of the volcanic system. Like most volcanoes, Moorea's topography has been deeply affected by various successions of building, destructive stages and by topographic inversions. Due to the field complexities, this volcanic system remains poorly understood, however our model explains the first order features consisting in (1) the building of a first shield; (2) a northern flank collapse; (3) a first localized filling of the central depression combined with the presence of decentralized small eruptive centers; (4) the filling of paleo-valleys all around the island; (5) the progressive end of volcanism and (6) the dismantlement of the residual volcano to this day while a coral reef has slowly been colonizing the shallow sea waters accommodating the island's subsidence and late quaternary eustatic variations. We leave open the possibility of other more hypothetical flank-collapses in the eastern or western areas which should be elucidated by a set of new analyses (e.g., fieldwork, geochronological, geophysical) in still poorly constrained areas (Vaiare, Haapiti, Papetoai). The understanding of Moorea's geology has crucial implications for local hydrogeological purposes.

CRediT authorship contribution statement

T. Bechon: Writing – review & editing, Writing – original draft, Visualization, Validation, Investigation, Formal analysis, Data curation, Conceptualization. **A. Hildenbrand:** Writing – review & editing, Writing – original draft, Visualization, Validation, Supervision, Resources, Methodology, Investigation, Formal analysis, Data curation, Conceptualization. **H. Pons:** Investigation, Data curation. **M. Dumont:** Writing – review & editing, Supervision, Investigation, Data curation. **P. Lachassagne:** Writing – review & editing, Supervision, Investigation, Conceptualization. **L. Sichoix:** Writing – review & editing, Supervision, Resources, Project administration, Methodology, Investigation, Funding acquisition, Data curation, Conceptualization.

Funding

This research has been supported by the Government of French Polynesia – Ministère de la Recherche (Project RESEAU Moorea, grant no. 7848/VP/REC 2021/10/04 and amendment 6437/MPR 2024/10/03), by a tripartite convention between the University of French Polynesia, the Moorea-Maiao Municipality and the Polynésienne des Eaux Company (grant no. UPF 22088 2023/06/26 and amendment UPF 24091 2025/01/13), and by the University of French Polynesia (Program "AAP post-doc 2025") to support the hiring of T. B. The three grants were awarded to L.S.. Airplanes tickets to France were paid by GEPASUD laboratory to T.B..

Declaration of competing interest

The authors declare that they have no known competing financial interests or personal relationships that could have appeared to influence the work reported in this paper.

Acknowledgments

The final version of the manuscript benefited from the constructive remarks from K. Nemeth and an anonymous reviewer, which improved the manuscript. We are grateful towards S. Cronin for editing the paper. The authors warmly thanks (1) staff members from the Municipality of Moorea-Maiao, the Polynésienne des Eaux company, the Delegation for Research of French Polynesia and the CRIOBE research station in Moorea for their supports, (2) Yuhji Yamamoto for sharing field data from Uto et al. (2007) that helped to locate their samples on the map, (3) Xavier Quidelleur, Jean-Claude Lefèvre, Pierre Lahitte for the practical help in the lab and the congenial coffees breaks, (4) Valérie Godard for the realization of the thin sections, (5) Puaitemarama Terai, Olivier Pôté and Vetea Hahe for direct support on the fieldwork, (6) all the Green Pearl Golf society for the passage and sampling authorizations or kart lending, (7) Bernard Capron (volunteer), Léon Harehoe (Municipality), Sean Labrunie (student), Lorelei Parau (student), Kimberley Pukeeinui (student), Garance Tanguy (Ph.D.), Antonio Teamo (inhabitant), Manutahi and Ronald Teariki (inhabitant or municipality), the Vaiho family (inhabitants), who joined or led us in the field (8) anonymous inhabitants of Moorea for various information, passage and sampling authorizations, discussions or dog restraining when necessary.

Appendix A. Supplementary data

Supplementary material related to this article can be found online at https://doi.org/10.1016/j.jvolgeores.2026.108555.

Data availability

Data will be made available on request.

References

Arrué, B.B., Rochlitz, R., Günther, T., Ronczka, M., Müller-Petke, M., 2024. Exploring groundwater salinization using drone-based electromagnetics in the North Sea Region, Germany. 2024, (1), European Association of Geoscientists & Engineers, pp. 1–5. http://dx.doi.org/10.3997/2214-4609.202420177, URL: https://www.earthdoc.org/content/papers/10.3997/2214-4609.202420177.

Baud, B., Lachassagne, P., Dumont, M., Toulier, A., Hendrayana, H., Fadillah, A., Dorfliger, N., 2024. Review: Andesitic aquifers—Hydrogeological conceptual models and insights relevant to applied hydrogeology. Hydrogeol. J. 32 (5), 1259–1286. http://dx.doi.org/10.1007/s10040-024-02784-0.

Becerril, L., Galindo, I., Martí, J., Gudmundsson, A., 2015. Three-armed rifts or masked radial pattern of eruptive fissures? The intriguing case of El Hierro volcano (Canary Islands). Tectonophysics 647–648, 33–47. http://dx.doi.org/10.1016/j.tecto.2015.02.006, URL: https://www.sciencedirect.com/science/article/pii/S0040195115000803.

Bellon, H., Blanchard, F., 1981. Aspects géochronologiques(K-Ar) de l'activité volcanique dans l'île de Moorea, Pacifique Central. Tectonophysics 72 (1), T33–T43. http://dx.doi.org/10.1016/0040-1951(81)90083-4, URL: https://www.sciencedirect.com/science/article/pii/0040195181900834.

Boulesteix, T., Hildenbrand, A., Gillot, P.-Y., Soler, V., 2012. Eruptive response of oceanic islands to giant landslides: New insights from the geomorphologic evolution of the Teide–Pico Viejo volcanic complex (Tenerife, Canary). Geomorphology 138 (1), 61–73. http://dx.doi.org/10.1016/j.geomorph.2011.08.025, URL: https://www.sciencedirect.com/science/article/pii/S0169555X11004466.

Boulesteix, T., Hildenbrand, A., Soler, V., Quidelleur, X., Gillot, P.-Y., 2013. Coeval giant landslides in the Canary Islands: Implications for global, regional and local triggers of giant flank collapses on oceanic volcanoes. J. Volcanol. Geotherm. Res. 257, 90–98. http://dx.doi.org/10.1016/j.jvolgeores.2013.03.008, URL: https://www.sciencedirect.com/science/article/pii/S0377027313000838.

Bret, L., Fevre, Y., Join, J.-L., Robineau, B., Bachelery, P., 2003. Deposits related to degradation processes on Piton des Neiges Volcano (Reunion Island): Overview and geological hazard. J. Volcanol. Geotherm. Res. 123 (1), 25–41. http://dx.doi.org/10.1016/S0377-0273(03)00026-X, URL: https://www.sciencedirect.com/science/article/pii/S037702730300026X.

Brousse, R., Boutault, G., Eisentein, A., Gelugne, P., 1985. Tahiti-Nui, carte géologique (1/25000), carte des formations de surface (1/25000), carte des instabilités et risques naturels (1/50000), feuille Papeete, Ministère de l'équipement, de l'aménagement, de l'énergie et des mines.

Brunet, M., Le Friant, A., Boudon, G., Lafuerza, S., Talling, P., Hornbach, M., Ishizuka, O., Lebas, E., Guyard, H., IODP Expedition 340 Science Party, 2016. Composition, geometry, and emplacement dynamics of a large volcanic island landslide offshore Martinique: From volcano flank-collapse to seafloor sediment failure? Geochem. Geophys. Geosyst. 17 (3), 699–724. http://dx.doi.org/10.1002/2015GC006034, URL: https://onlinelibrary.wiley.com/doi/abs/10.1002/2015GC006034.

Carracedo, J.C., Day, S.J., Guillou, H., Pérez Torrado, F.J., 1999. Giant quaternary landslides in the evolution of La Palma and El Hierro, Canary Islands. J. Volcanol. Geotherm. Res. 94 (1), 169–190. http://dx.doi.org/10.1016/S0377-0273(99)00102-X, URL: https://www.sciencedirect.com/science/article/pii/S037702739900102X.

Casalbore, D., Romagnoli, C., Bosman, A., Chiocci, F.L., 2011. Potential tsunamigenic landslides at Stromboli Volcano (Italy): Insight from marine DEM analysis. Geomorphology 126 (1), 42–50. http://dx.doi.org/10.1016/j.geomorph.2010.10.026, URL: https://www.sciencedirect.com/science/article/pii/S0169555X10004642.

Clouard, V., Bonneville, A., 2005. Ages of seamounts, islands, and plateaus on the Pacific plate. In: Foulger, G.R., Natland, J.H., Presnall, D.C., Anderson, D.L. (Eds.), Plates, Plumes and Paradigms. Geological Society of America, http://dx.doi.org/10.1130/0-8137-2388-4.71.

Clouard, V., Bonneville, A., Barsczus, H.G., 2000. Size and depth of ancient magma reservoirs under atolls and islands of French Polynesia using gravity data. J. Geophys. Res.: Solid Earth 105 (B4), 8173–8191. http://dx.doi.org/10.1029/1999JB900393, URL: https://onlinelibrary.wiley.com/doi/abs/10.1029/1999JB900393.

Clouard, V., Bonneville, A., Gillot, P.-Y., 2001. A giant landslide on the southern flank of Tahiti Island, French Polynesia. Geophys. Res. Lett. 28 (11), 2253–2256. http://dx.doi.org/10.1029/2000GL012604, URL: https://onlinelibrary.wiley.com/doi/abs/10.1029/2000GL012604.

Costa, A.C.G., Hildenbrand, A., Marques, F.O., Sibrant, A.L.R., Santos de Campos, A., 2015. Catastrophic flank collapses and slumping in Pico Island during the last 130 Kyr (Pico-Faial ridge, Azores Triple Junction). J. Volcanol. Geotherm. Res. 302, 33–46. http://dx.doi.org/10.1016/j.jvolgeores.2015.06.008, URL: https://www.sciencedirect.com/science/article/pii/S0377027315001845.

Costa, A.C.G., Marques, F.O., Hildenbrand, A., Sibrant, A.L.R., Catita, C.M.S., 2014. Large-scale catastrophic flank collapses in a steep volcanic ridge: The Pico–Faial Ridge, Azores Triple Junction. J. Volcanol. Geotherm. Res. 272, 111–125. http://dx.doi.org/10.1016/j.jvolgeores.2014.01.002, URL: https://www.sciencedirect.com/science/article/pii/S0377027314000109.

Deneufbourg, G., 1962. Rapport Spécial Sur La Reconnaissance Géologique Générale de l'île de Moorea. Technical Report, BRGM, p. 29.

Diraison, C., Bellon, H., Leotot, C., Brousse, R., Barsczus, H.G., 1991. L'alignement de la société (Polynésie Française) : Volcanologie, géochronologie, proposition d'un modèle de point chaud. Bull. Soc. Géol. Fr. t. 162 (3), 479–496.

Dondin, F., Lebrun, J.-F., Kelfoun, K., Fournier, N., Randrianasolo, A., 2012. Sector collapse at Kick 'em Jenny submarine volcano (Lesser Antilles): Numerical simulation and landslide behaviour. Bull. Volcanol. 74 (2), 595–607. http://dx.doi.org/10.1007/s00445-011-0554-0.

Duffield, W.A., Stieltjes, L., Varet, J., 1982. Huge landslide blocks in the growth of piton de la fournaise, La réunion, and Kilauea volcano, Hawaii. J. Volcanol. Geotherm. Res. 12 (1), 147–160. http://dx.doi.org/10.1016/0377-0273(82)90009-9, URL: https://www.sciencedirect.com/science/article/pii/0377027382900099.

Dumont, M., Reninger, P.A., Aunay, B., Pryet, A., Jougnot, D., Join, J.L., Michon, L., Martelet, G., 2021. Hydrogeophysical characterization in a volcanic context from local to regional scales combining airborne electromagnetism and magnetism. Geophys. Res. Lett. 48 (12), e2020GL092000. http://dx.doi.org/10.1029/2020GL092000, URL: https://onlinelibrary.wiley.com/doi/abs/10.1029/2020GL092000.

Duncan, R.A., McDougall, I., 1976. Linear volcanism in French Polynesia. J. Volcanol. Geotherm. Res. 1 (3), 197–227. http://dx.doi.org/10.1016/0377-0273(76)90008-1, URL: https://www.sciencedirect.com/science/article/pii/0377027376900081.

Fadil, A., Sichoix, L., Barriot, J.-P., Ortéga, P., Willis, P., 2011. Evidence for a slow subsidence of the Tahiti island from GPS, DORIS, and combined satellite altimetry and tide gauge sea level records. C. R. Géosci. 343 (5), 331–341. http://dx.doi.org/10.1016/j.crte.2011.02.002, URL: https://comptes-rendus.academie-sciences.fr/geoscience/articles/10.1016/j.crte.2011.02.002/.

Garner, E.L., Murphy, T.J., Gramlich, J.W., Paulsen, P.J., Barnes, I.L., 1975. Absolute isotopic abundance ratios and the atomic weight of a reference sample of potassium. J. Res. Natl. Bur. Stand. Sect. A, Phys. Chem. 79A (6), 713. http://dx.doi.org/10.6028/jres.079A.028, arXiv:32184525. URL: https://pmc.ncbi.nlm.nih.gov/articles/PMC6589417/.

Germa, A., Quidelleur, X., Labanieh, S., Chauvel, C., Lahitte, P., 2011a. The volcanic evolution of Martinique Island: Insights from K–Ar dating into the lesser antilles arc migration since the Oligocene. J. Volcanol. Geotherm. Res. 208 (3), 122–135. http://dx.doi.org/10.1016/j.jvolgeores.2011.09.007, URL: https://www.sciencedirect.com/science/article/pii/S0377027311002502.

Germa, A., Quidelleur, X., Lahitte, P., Labanieh, S., Chauvel, C., 2011b. The K–Ar Cassignol–Gillot technique applied to western Martinique lavas: A record of Lesser Antilles arc activity from 2Ma to Mount Pelée volcanism. Quat. Geochronol. 6 (3), 341–355. http://dx.doi.org/10.1016/j.quageo.2011.02.001, URL: https://www.sciencedirect.com/science/article/pii/S1871101411000082.

Gillot, P.-Y., Albore-Livadie, C., Lefèvre, J.-C., Hildebrand, A., 2006. The K/Ar dating method : Principle, analytical techniques, and application to holocene volcanic eruptions in Southern Italy. Acta Vulcanol. : J. Natl. Volcan. Group Italy 1000–1011. http://dx.doi.org/10.1400/93820, 18, 1/2, 2006. URL: https://www.torrossa.com/en/resources/an/2231647.

Gillot, P.-Y., Cornette, Y., Max, N., Floris, B., 1992. Two reference materials, trachytes Mdo-G and Ish-G, for argon dating (k-Ar and 40ar/39ar) of pleistocene and holocene rocks. Geostand. Newsl. 16 (1), 55–60. http://dx.doi.org/10.1111/j.1751-908X.1992.tb00487.x, URL: https://onlinelibrary.wiley.com/doi/abs/10.1111/j.1751-908X.1992.tb00487.x.

Gillot, P.-Y., Lefèvre, J.-C., Nativel, P.-E., 1994. Model for the structural evolution of the volcanoes of Réunion Island. Earth Planet. Sci. Lett. 122 (3), 291–302. http://dx.doi.org/10.1016/0012-821X(94)90003-5, URL: https://www.sciencedirect.com/science/article/pii/0012821X94900035.

Guillou, H., Blais, S., Guille, G., Maury, R.C., Dez, A.L., Cotten, J., 1998. Ages (K-Ar) et durées d'édification subaérienne des îles de Moorea, raiatea et maupiti (société, polynésie française). Géol. Fr. 3, 3, URL: https://hal.science/hal-03323409.

Guillou, H., Maury, R.C., Blais, S., Cotten, J., Legendre, C., Guille, G., Caroff, M., 2005. Age progression along the Society hotspot chain (French Polynesia) based on new unspiked K-Ar ages. Bull. Soc. Géol. Fr. 176 (2), 135–150. http://dx.doi.org/10.2113/176.2.135.

Hevia-Cruz, F., Hildenbrand, A., Sheldon, N.D., Chabaux, F., Marques, F.O., Carlut, J., 2025. Fast CO2 uptake by intense weathering of volcanic islands during interglacial stages. Geochim. Cosmochim. Acta 401, 62–76. http://dx.doi.org/10.1016/j.gca.2025.05.035, URL: https://www.sciencedirect.com/science/article/pii/S0016703725002881.

Hevia-Cruz, F., Hildenbrand, A., Sheldon, N.D., Hren, M.T., Zanon, V., Marques, F.O., Carlut, J., Chabaux, F., Haurine, F., 2024a. Weathering pulses during glacial-interglacial transitions: Insights from well-dated paleosols in the Azores volcanic province (Central North Atlantic). Quat. Sci. Rev. 324, 108438. http://dx.doi.org/10.1016/j.quascirev.2023.108438, URL: https://www.sciencedirect.com/science/article/pii/S0277379123004869.

Hevia-Cruz, F., Sheldon, N.D., Hildenbrand, A., Hren, M.T., Marques, F.O., Carlut, J., Chabaux, F., 2024b. Regional Variations of the Azores High Across Glacial-Interglacial Timescales. Paleoceanogr. Paleoclimatol. 39 (5), e2023PA004810. http://dx.doi.org/10.1029/2023PA004810, URL: https://onlinelibrary.wiley.com/doi/abs/10.1029/2023PA004810.

Hildenbrand, A., Gillot, P.-Y., Bonneville, A., 2006. Offshore evidence for a huge landslide of the northern flank of Tahiti-Nui (French Polynesia). Geochem. Geophys. Geosyst. 7 (3), http://dx.doi.org/10.1029/2005GC001003, URL: https://onlinelibrary.wiley.com/doi/abs/10.1029/2005GC001003.

Hildenbrand, A., Gillot, P.-Y., Le Roy, I., 2004. Volcano-tectonic and geochemical evolution of an oceanic intra-plate volcano: Tahiti-Nui (French Polynesia). Earth Planet. Sci. Lett. 217 (3), 349–365. http://dx.doi.org/10.1016/S0012-821X(03)00599-5, URL: https://www.sciencedirect.com/science/article/pii/S0012821X03005995.

Hildenbrand, A., Gillot, P.-Y., Marlin, C., 2008. Geomorphological study of long-term erosion on a tropical volcanic ocean island: Tahiti-Nui (French Polynesia). Geomorphology 93 (3), 460–481. http://dx.doi.org/10.1016/j.geomorph.2007.03.012, URL: https://www.sciencedirect.com/science/article/pii/S0169555X07001109.

Hildenbrand, A., Gillot, P.-Y., Soler, V., Lahitte, P., 2003. Evidence for a persistent uplifting of La Palma (Canary Islands), inferred from morphological and radiometric data. Earth Planet. Sci. Lett. 210 (1), 277–289. http://dx.doi.org/10.1016/S0012-821X(03)00133-X, URL: https://www.sciencedirect.com/science/article/pii/S0012821X0300133X.

Hildenbrand, A., Marlin, C., Conroy, A., Gillot, P.-Y., Filly, A., Massault, M., 2005. Isotopic approach of rainfall and groundwater circulation in the volcanic structure of Tahiti-Nui (French Polynesia). J. Hydrol. 302 (1), 187–208. http://dx.doi.org/10.1016/j.jhydrol.2004.07.006, URL: https://www.sciencedirect.com/science/article/pii/S0022169404003841.

Hildenbrand, A., Marques, F.O., Catalão, J., 2018. Large-scale mass wasting on small volcanic islands revealed by the study of Flores Island (Azores). Sci. Rep. 8 (1), 13898. http://dx.doi.org/10.1038/s41598-018-32253-0, URL: https://www.nature.com/articles/s41598-018-32253-0.

Hildenbrand, A., Marques, F.O., Costa, A.C.G., Sibrant, A.L.R., Silva, P.F., Henry, B., Miranda, J.M., Madureira, P., 2012. Reconstructing the architectural evolution of volcanic islands from combined K/Ar, morphologic, tectonic, and magnetic data: The Faial Island example (Azores). J. Volcanol. Geotherm. Res. 241–242, 39–48. http://dx.doi.org/10.1016/j.jvolgeores.2012.06.019, URL: https://www.sciencedirect.com/science/article/pii/S0377027312001874.

Hildenbrand, A., Marques, F.O., Pereira, A., Nomade, S., Hevia-Cruz, F., 2024. Precise dating of large flank collapses by single-grain 40Ar/39Ar on pyroclastic deposits from the example of Flores Island (Azores). Sci. Rep. 14 (1), 11905. http://dx.doi.org/10.1038/s41598-024-62583-1, URL: https://www.nature.com/articles/s41598-024-62583-1.

Izquierdo, T., 2014. Conceptual hydrogeological model and aquifer system classification of a small volcanic island (La Gomera; Canary Islands). CATENA 114, 119–128. http://dx.doi.org/10.1016/j.catena.2013.11.006, URL: https://www.sciencedirect.com/science/article/pii/S0341816213002762.

Jamet, 2000. Les Sols de Moorea et Des Îles Sous-le-Vent.. Technical Report, Editions de l'institut de Recherche pour le Développement (IRD), URL: https://horizon.documentation.ird.fr/exl-doc/pleins_textes/pleins_textes_5/notexp/010022564.pdf.

Jefferson, A.J., Ferrier, K.L., Perron, J.T., Ramalho, R., 2014. Controls on the hydrological and topographic evolution of shield volcanoes and volcanic ocean islands. In: The Galápagos. American Geophysical Union (AGU), pp. 185–213. http://dx.doi.org/10.1002/9781118852538.ch10, URL: https://onlinelibrary.wiley.com/doi/abs/10.1002/9781118852538.ch10.

Keating, B.H., McGuire, W.J., 2000. Island edifice failures and associated tsunami hazards. Pure Appl. Geophys. 157 (6), 899–955. http://dx.doi.org/10.1007/s000240050011.

Kelley, S., 2002. Excess argon in K–Ar and Ar–Ar geochronology. Chem. Geol. 188 (1), 1–22. http://dx.doi.org/10.1016/S0009-2541(02)00064-5, URL: https://www.sciencedirect.com/science/article/pii/S0009254102000645.

Kirch, P.V., Kahn, J.G., Chadwick, O.A., 2023. Soils, agriculture, and land use in island socio-ecosystems: Three case studies from Southeastern Polynesia. Geoarchaeology 38 (1), 20–34. http://dx.doi.org/10.1002/gea.21934, URL: https://onlinelibrary.wiley.com/doi/abs/10.1002/gea.21934.

Lachassagne, P., Aunay, B., Frissant, N., Guilbert, M., Malard, A., 2014. High-resolution conceptual hydrogeological model of complex basaltic volcanic islands: A Mayotte, Comoros, case study. Terra Nova 26 (4), 307–321. http://dx.doi.org/10.1111/ter.12102, URL: https://onlinelibrary.wiley.com/doi/abs/10.1111/ter.12102.

Le Dez, A., 1996. Variations pétrologiques et géochimiques associées à l'édification des volcans-boucliers de Polynesie française : Exemples de Nuku Hiva et Hiva Oa (Marquises) et de Moorea (Société), Ph.D. thesis. URL: https://theses.fr/1996BRES2012.

Le Dez, A., Maury, R.C., Guillou, H., Cotten, J., Blais, S., Guille, G., 1998. L'île de Moorea (société) : Édification rapide d'un volcan-bouclier polynésien. Géol. Fr. 3, 51, URL: https://hal.science/hal-03323410.

Le Friant, A., Boudon, G., Deplus, C., Villemant, B., 2003. Large-scale flank collapse events during the activity of Montagne Pelée, Martinique, Lesser Antilles. J. Geophys. Res.: Solid Earth 108 (B1), http://dx.doi.org/10.1029/2001JB001624, URL: https://onlinelibrary.wiley.com/doi/abs/10.1029/2001JB001624.

Le Roy, I., 1994. The evolution of hot spot volcanoes: The island of Tahiti, society archipelago (French polynesia), Ph.D. thesis. URL: https://inis.iaea.org/records/h8hq4-wwe71.

Loiodice, L., Hevia-Cruz, F., Hildenbrand, A., Sheldon, N.D., 2025. Unexpected wet and warm conditions during glacial periods in the Central North Atlantic as recorded by paleosols from Flores Island (Western Azores). Palaeogeogr. Palaeoclimatol. Palaeoecol. 676, 113157. http://dx.doi.org/10.1016/j.palaeo.2025.113157, URL: https://www.sciencedirect.com/science/article/pii/S0031018225004420.

Manconi, A., Longpré, M.-A., Walter, T.R., Troll, V.R., Hansteen, T.H., 2009. The effects of flank collapses on volcano plumbing systems. Geology 37 (12), 1099–1102. http://dx.doi.org/10.1130/G30104A.1.

Marazuela, M.Á., Baquedano, C., Cruz-Pérez, N., Martínez-León, J., Laspidou, C., Santamarta, J.C., García-Gil, A., 2023. Dyke-impounded fresh groundwater resources in coastal and island volcanic aquifers: Learning from the Canary Islands (Spain). Sci. Total Environ. 899, 165638. http://dx.doi.org/10.1016/j.scitotenv.2023.165638, URL: https://www.sciencedirect.com/science/article/pii/S0048969723042614.

Marques, F.O., Catalão, J., Hübscher, C., Costa, A.C.G., Hildenbrand, A., Zeyen, H., Nomikou, P., Lebas, E., Zanon, V., 2021. The shaping of a volcanic ridge in a tectonically active setting: The Pico-Faial Ridge in the Azores Triple Junction. Geomorphology 378, 107612. http://dx.doi.org/10.1016/j.geomorph.2021.107612, URL: https://www.sciencedirect.com/science/article/pii/S0169555X21000210.

Marques, F.O., Hildenbrand, A., Victória, S.S., Cunha, C., Dias, P., 2019. Caldera or flank collapse in the Fogo volcano? What age? Consequences for risk assessment in volcanic islands. J. Volcanol. Geotherm. Res. 388, 106686. http://dx.doi.org/10.1016/j.jvolgeores.2019.106686, URL: https://www.sciencedirect.com/science/article/pii/S0377027319301787.

Marques, F.O., Ribeiro, L.P., Hübscher, C., Costa, A.C.G., Hildenbrand, A., 2025. How and why small volcanic ocean islands collapse and move vertically up and down. Sci. Rep. 15 (1), 3835. http://dx.doi.org/10.1038/s41598-025-87191-5, URL: https://www.nature.com/articles/s41598-025-87191-5.

Masson, D.G., Le Bas, T.P., Grevemeyer, I., Weinrebe, W., 2008. Flank collapse and large-scale landsliding in the Cape Verde Islands, off West Africa. Geochem. Geophys. Geosyst. 9 (7), http://dx.doi.org/10.1029/2008GC001983, URL: https://onlinelibrary.wiley.com/doi/abs/10.1029/2008GC001983.

Masson, D.G., Watts, A.B., Gee, M.J.R., Urgeles, R., Mitchell, N.C., Le Bas, T.P., Canals, M., 2002. Slope failures on the flanks of the western Canary Islands. Earth-Sci. Rev. 57 (1), 1–35. http://dx.doi.org/10.1016/S0012-8252(01)00069-1, URL: https://www.sciencedirect.com/science/article/pii/S0012825201000691.

Maury, R.C., Guille, G., Guillou, H., Chauvel, C., Legendre, C., Rossi, P., Blais, S., Pallares, C., Deroussi, S., Anne-Marie, M., 2014. Géologie des marquises : Des volcans boucliers intra-océaniques effondrés issus d'un point chaud atypique. Géol. Fr. (1), 111, URL: https://insu.hal.science/insu-01096396.

Maury, R.-C., Le Dez, A., Guillou, H., 2000. Carte géologique de France (1/25000), feuille de Moorea - Polynésie-Française. BRGM, notice 62 p.

McDougall, I., Harrison, T.M., 1999. Geochronology and Theromochronology By The 40 Ar/39 Ar Method. Oxford University Press, http://dx.doi.org/10.1093/oso/9780195109207.001.0001, URL: https://academic.oup.com/book/53774.

Miller, C.A., Schaefer, L.N., Kereszturi, G., Fournier, D., 2020. Three-dimensional mapping of Mt. Ruapehu Volcano, new zealand, from aeromagnetic data inversion and hyperspectral imaging. J. Geophys. Res.: Solid Earth 125 (2), e2019JB018247. http://dx.doi.org/10.1029/2019JB018247, URL: https://onlinelibrary.wiley.com/doi/abs/10.1029/2019JB018247.

Moore, J.G., Clague, D.A., Holcomb, R.T., Lipman, P.W., Normark, W.R., Torresan, M.E., 1989. Prodigious submarine landslides on the Hawaiian Ridge. J. Geophys. Res.: Solid Earth 94 (B12), 17465–17484. http://dx.doi.org/10.1029/JB094iB12p17465, URL: https://onlinelibrary.wiley.com/doi/abs/10.1029/JB094iB12p17465.

Navarro, J.M., Coello, J., 1993. Sucesión de episodios en la evolución geológica de la palma. Mapa geológico de la palma. Geological map.

Németh, K., Gravis, I., 2022. Geoheritage and geodiversity elements of the SW Pacific: A conceptual framework. Int. J. Geoheritage Park. 10 (4), 523–545. http://dx.doi.org/10.1016/j.ijgeop.2022.09.001, URL: https://www.sciencedirect.com/science/article/pii/S257744412200065X.

Németh, K., Zakharovskyi, V., 2025. Geodiversity of Samoa. In: Németh, K., Zakharovskyi, V. (Eds.), Geodiversity of Samoa: An Untapped and Unique Geoheritage Hot Spot in the Southwestern Pacific. Springer Nature Switzerland, pp. 95–125. http://dx.doi.org/10.1007/978-3-031-87220-4_3.

Niyazi, Y., Stewart, H.A., Harrison, D., Jamieson, A.J., Bond, T., 2025. Submarine landslides along the flanks of Christmas Island, Indian ocean. Geo-Marine Lett. 45 (4), 36. http://dx.doi.org/10.1007/s00367-025-00821-9.

Oehler, J.-F., van Wyk de Vries, B., Labazuy, P., 2005. Landslides and spreading of oceanic hot-spot and arc shield volcanoes on low strength layers (LSLs): An analogue modeling approach. J. Volcanol. Geotherm. Res. 144 (1), 169–189. http://dx.doi.org/10.1016/j.jvolgeores.2004.11.023, URL: https://www.sciencedirect.com/science/article/pii/S0377027304004263.

Ogg, J., 2020. Geomagnetic Polarity Time Scale. In: Gradstein, F.M., Ogg, J.G., Schmitz, M.D., Ogg, G.M. (Eds.), Geologic Time Scale 2020. Elsevier, Amsterdam, pp. 159–192. http://dx.doi.org/10.1016/B978-0-12-824360-2.00005-X.

Quesada-Román, A., Peralta-Reyes, M., Németh, K., Tefogoum, G.Z., Dóniz-Páez, J., Zwoliński, Z., da Glória Motta Garcia, M., Mazurek, M., Migoń, P., 2025. Geoheritage of tropical regions: An overview. Int. J. Geoheritage Park. 13 (3), 388–411. http://dx.doi.org/10.1016/j.ijgeop.2025.05.004, URL: https://www.sciencedirect.com/science/article/pii/S2577444125000395.

Quidelleur, X., Famin, V., 2024. Last 150 Kyr volcanic activity on Mauritius island (Indian ocean) revealed by new Cassignol-Gillot unspiked K–Ar ages. Quat. Geochronol. 82, 101534. http://dx.doi.org/10.1016/j.quageo.2024.101534, URL: https://www.sciencedirect.com/science/article/pii/S1871101424000384.

Quidelleur, X., Gillot, P.-Y., Carlut, J., Courtillot, V., 1999. Link between excursions and paleointensity inferred from abnormal field directions recorded at La Palma around 600 Ka. Earth Planet. Sci. Lett. 168 (3), 233–242. http://dx.doi.org/10.1016/S0012-821X(99)00061-8, URL: https://www.sciencedirect.com/science/article/pii/S0012821X99000618.

Quidelleur, X., Hildenbrand, A., Samper, A., 2008. Causal link between quaternary paleoclimatic changes and volcanic islands evolution. Geophys. Res. Lett. 35 (2), http://dx.doi.org/10.1029/2007GL031849, URL: https://onlinelibrary.wiley.com/doi/abs/10.1029/2007GL031849.

Raczek, I., Stoll, B., Hofmann, A.W., Peter Jochum, K., 2001. High-precision trace element data for the USGS reference materials BCR-1, BCR-2, BHVO-1, BHVO-2, AGV-1, AGV-2, DTS-1, DTS-2, GSP-1 and GSP-2 by ID-TIMS and MIC-SSMS. Geostand. Newsl. 25 (1), 77–86. http://dx.doi.org/10.1111/j.1751-908X.2001.tb00789.x, URL: https://onlinelibrary.wiley.com/doi/abs/10.1111/j.1751-908X.2001.tb00789.x.

Ricci, J., Carlut, J., Marques, F.O., Hildenbrand, A., Valet, J.-P., 2020. Volcanic record of the last geomagnetic reversal in a lava flow sequence from the azores. Front. Earth Sci. Volume 8 - 2020, URL: https://www.frontiersin.org/journals/earth-science/articles/10.3389/feart.2020.00165.

Rougeau, S., Quidelleur, X., Famin, V., Michon, L., Nauret, F., Rusquet, A., Di Muro, A., Famin, V., Michon, L., Nauret, F., Rusquet, A., Di Muro, A., 2024. Reconstruction de l'histoire volcanique de la Grande Comore et implications volcano-tectoniques pour l'archipel des Comores. C. R. Geosci. 357 (G1), 125–144. http://dx.doi.org/10.5802/crgeos.292, URL: https://archimer.ifremer.fr/doc/00956/106825/.

Schaen, A.J., Jicha, B.R., Hodges, K.V., Vermeesch, P., Stelten, M.E., Mercer, C.M., Phillips, D., Rivera, T.A., Jourdan, F., Matchan, E.L., Hemming, S.R., Morgan, L.E., Kelley, S.P., Cassata, W.S., Heizler, M.T., Vasconcelos, P.M., Benowitz, J.A., Koppers, A.A., Mark, D.F., Niespolo, E.M., Sprain, C.J., Hames, W.E., Kuiper, K.F., Turrin, B.D., Renne, P.R., Ross, J., Nomade, S., Guillou, H., Webb, L.E., Cohen, B.A., Calvert, A.T., Joyce, N., Ganerød, M., Wijbrans, J., Ishizuka, O., He, H., Ramirez, A., Pfänder, J.A., Lopez-Martínez, M., Qiu, H., Singer, B.S., 2020. Interpreting and reporting 40Ar/39Ar geochronologic data. GSA Bull. 133 (3–4), 461–487. http://dx.doi.org/10.1130/B35560.1.

Schwarz, W.H., Trieloff, M., 2007. Intercalibration of 40Ar–39Ar age standards NL-25, HB3gr hornblende, GA1550, SB-3, HD-B1 Biotite and BMus/2 muscovite. Chem. Geol. 242 (1), 218–231. http://dx.doi.org/10.1016/j.chemgeo.2007.03.016, URL: https://www.sciencedirect.com/science/article/pii/S0009254107001490.

Shih, H.-C., Hwang, C., Barriot, J.-P., Mouyen, M., Corréia, P., Lequeux, D., Sichoix, L., 2015. High-resolution gravity and geoid models in Tahiti obtained from new airborne and land gravity observations: Data fusion by spectral combination. Earth, Planets Space 67 (1), 124. http://dx.doi.org/10.1186/s40623-015-0297-9.

Sibrant, A.L.R., Hildenbrand, A., Marques, F.O., Costa, A.C.G., 2015a. Volcano-tectonic evolution of the Santa Maria Island (Azores): Implications for paleostress evolution at the western Eurasia–Nubia plate boundary. J. Volcanol. Geotherm. Res. 291, 49–62. http://dx.doi.org/10.1016/j.jvolgeores.2014.12.017, URL: https://www.sciencedirect.com/science/article/pii/S0377027314003989.

Sibrant, A.L.R., Hildenbrand, A., Marques, F.O., Weiss, B., Boulesteix, T., Hübscher, C., Lüdmann, T., Costa, A.C.G., Catalão, J.C., 2015b. Morpho-structural evolution of a volcanic island developed inside an active oceanic rift: S. Miguel Island (Terceira Rift, Azores). J. Volcanol. Geotherm. Res. 301, 90–106. http://dx.doi.org/10.1016/j.jvolgeores.2015.04.011, URL: https://www.sciencedirect.com/science/article/pii/S0377027315001262.

Siebert, L., Reid, M.E., 2023. Lateral edifice collapse and volcanic debris avalanches: A post-1980 Mount St. Helens perspective. Bull. Volcanol. 85 (11), 61. http://dx.doi.org/10.1007/s00445-023-01662-z.

Singer, B.S., 2014. A quaternary geomagnetic instability time scale. Quat. Geochronol. 21, 29–52. http://dx.doi.org/10.1016/j.quageo.2013.10.003, URL: https://www.sciencedirect.com/science/article/pii/S1871101413000939.

Son, Y.-S., Noh, S.-G., Bang, E.-S., Kim, K.-E., Cho, S.-J., Baik, H., 2022. Ground-based visible–near infrared hyperspectral imaging for monitoring cliff weathering of a volcanic island in Dokdo, South Korea. Eng. Geol. 309, 106854. http://dx.doi.org/10.1016/j.enggeo.2022.106854, URL: https://www.sciencedirect.com/science/article/pii/S0013795222003398.

Steiger, R.H., Jäger, E., 1977. Subcommission on geochronology: Convention on the use of decay constants in geo- and cosmochronology. Earth Planet. Sci. Lett. 36 (3), 359–362. http://dx.doi.org/10.1016/0012-821X(77)90060-7, URL: https://www.sciencedirect.com/science/article/pii/0012821X77900607.

Terry, J.P., Goff, J., 2013. One hundred and thirty years since Darwin: 'Reshaping' the theory of atoll formation. Holocene 23 (4), 615–619. http://dx.doi.org/10.1177/0959683612463101.

Thomas, A.L., Fujita, K., Iryu, Y., Bard, E., Cabioch, G., Camoin, G., Cole, J.E., Deschamps, P., Durand, N., Hamelin, B., Heindel, K., Henderson, G.M., Mason, A.J., Matsuda, H., Ménabréaz, L., Omori, A., Quinn, T., Sakai, S., Sato, T., Sugihara, K., Takahashi, Y., Thouveny, N., Tudhope, A.W., Webster, J., Westphal, H., Yokoyama, Y., 2012. Assessing subsidence rates and paleo water-depths for Tahiti reefs using U–Th chronology of altered corals. Mar. Geol. 295–298, 86–94. http://dx.doi.org/10.1016/j.margeo.2011.12.006, URL: https://www.sciencedirect.com/science/article/pii/S0025322711002970.

Toulier, A., Baud, B., de Montety, V., Lachassagne, P., Leonardi, V., Pistre, S., Dautria, J.-M., Hendrayana, H., Miftakhul Fajar, M.H., Satrya Muhammad, A., Beon, O., Jourde, H., 2019. Multidisciplinary study with quantitative analysis of isotopic data for the assessment of recharge and functioning of volcanic aquifers: Case of Bromo-Tengger volcano, Indonesia. J. Hydrol.: Reg. Stud. 26, 100634. http://dx.doi.org/10.1016/j.ejrh.2019.100634, URL: https://www.sciencedirect.com/science/article/pii/S2214581819300941.

Uto, K., Yamamoto, Y., Sudo, M., Uchiumi, S., Ishizuka, O., Kogiso, T., Tsunakawa, H., 2007. New K-Ar ages of the Society Islands, French Polynesia, and implications for the Society hotspot feature. Earth, Planets Space 59 (7), 879–885. http://dx.doi.org/10.1186/BF03352750.

Walter, T.R., Troll, V.R., 2003. Experiments on rift zone evolution in unstable volcanic edifices. J. Volcanol. Geotherm. Res. 127 (1), 107–120. http://dx.doi.org/10.1016/S0377-0273(03)00181-1, URL: https://www.sciencedirect.com/science/article/pii/S0377027303001811.